NATIONAL ADVISORY COMMITTEE FOR AERONAUTICS

TECHNICAL NOTE 4291

AN EVALUATION OF EFFECTS OF FLEXIBILITY ON WING STRAINS

IN RÔUGH AIR FOR A LARGE SWEPT-WING AIRPLANE BY MEANS

OF EXPERIMENTALLY DETERMINED FREQUENCY-RESPONSE

FUNCTIONS WITH AN ASSESSMENT OF RANDOM-PROCESS

TECHNIQUES EMPLOYED

By Thomas L. Coleman, Harry Press, and May T. Meadows

Langley Aeronautical Laboratory
Langley Field, Va.

NACA

Washington

July 1958

.B

NACA TN 4291

CONTENTS

NATIONAL ADVISORY COMMITTEE FOR AERONAUTICS

TECHNICAL NOTE 4291

AN EVALUATION OF EFFECTS OF FLEXIBILITY ON WING STRAINS

IN ROUGH AIR FOR A LARGE SWEPT-WING AIRPLANE BY MEANS

OF EXPERIMENTALLY DETERMINED FREQUENCY-RESPONSE

FUNCTIONS WITH AN ASSESSMENT OF RANDOM-PROCESS

TECHNIQUES EMPLOYED

By Thomas L. Coleman, Harry Press, and May T. Meadows

SUMMARY

Power spectral methods of analysis are applied to flight test meas-
urements of the strain responses of a large swept-wing bomber airplane in
rough air in order to determine the effects of airplane structural dynamics
on the strain responses. Power spectra and frequency-response functions of
the strain responses are determined and compared with the estimated results
for a quasi-static reference airplane condition. The results obtained
indicate that the bending and shear strain responses are significantly
amplified in rough air because of the effect of structural dynamics by an
amount that varies from 10 to 20 percent at the root to about 100 percent
at the midspan station. The amplifications appear to be larger for the
high-altitude tests than for the low-altitude tests. The amplifications
of strains appear to be predominantly associated with the excitation of
the first wing-bending mode, although at the outboard stations and partic-
ularly for the shear strains significant effects also are introduced by
high-frequency structural modes.

The determination of airplane frequency-response functions for
responses to atmospheric turbulence from measurements in continuous
rough air involves a relatively new application of random-process tech-
niques. The results obtained appear to be subject to errors from a wide
number of sources which give rise to distortions and sampling errors.
A general analysis of the reliability of such frequency-response function
estimates is presented and methods of estimating the distortions and
sampling errors are developed. These methods are applied to the data in
order to establish the reliability of the present results. The results
indicate that with due precaution reliable estimates of frequency-response
functions can be obtained.

INTRODUCTION

The effects of airplane flexibility on the airplane loads and structural strains due to rough air are of major concern in the design of many modern airplanes. This subject has been under continual study during at least the past decade, and many useful results have been obtained both in experimental and analytical studies. For the case of large unswept-wing airplanes in subsonic flight, experimental studies (refs. 1 to 3) have indicated that the effects of flexibility could give rise to substantial amplifications in the strains in rough air. In addition, analytic studies based on power spectral techniques incorporating relatively simple aeroelastic analysis involving one or two symmetrical wing-bending modes have yielded good correlation with the flight-test results. (See refs. 4 and 5.)

With the increase of speeds into the high subsonic and supersonic regions and the associated introduction of new plan forms, particularly swept wings, the problems of aeroelastic response become both more important and more complex. For these airplanes, static aeroelastic deformations give rise to significant changes in the airplane aerodynamics and stability. In addition, the dynamic aeroelastic behavior may be expected to involve significant aerodynamic twist due to bending.

As a part of the investigation of the aeroelastic behavior of swept wings in rough air, a flight investigation involving a large flexible swept-wing airplane was recently undertaken. The initial results obtained on the overall effects of wing flexibility on the strains as measured by the root-mean-square strain values and counts of peak strains have been presented in references 6 and 7. In addition, a few initial experimentally determined frequency-response functions for the wing-bending strain responses are given in reference 8. The present paper extends the results of references 6 to 8 and presents a more comprehensive treatment of the flight-test results in regard to the effects of aeroelasticity on the structural strains in rough air.

One of the objectives of the present analysis is the evaluation of the effects of airplane flexibility on the wing strain responses to vertical gusts. For this purpose, power spectra of the measured strain responses at various spanwise stations are determined and compared with the estimated strain power spectra for a quasi-static reference airplane condition. However, the measured power spectra appear to be subject to errors arising from the effects of extraneous "noises" such as strain responses due to side gusts and the effects of reading errors. Therefore, the test measurements were also used in order to determine the frequency-response functions for the strain responses to vertical gusts. These frequency-response functions are also compared with the strain frequency-response functions for a quasi-static reference condition in order to

establish the effects of the dynamic flexibility on the strains in a more
reliable manner. The frequency-response functions appear to be less sen-
sitive to the effects of noise, to describe the response characteristics
of the airplane independently of the gust input, and also to have a num-
ber of other applications; they may be directly compared with the results
of analytic calculations and thus serve as a guide to the reliability of
such calculations; and they may be used for computing responses to arbi-
trary gust inputs of a specified or random nature.

A second objective of the present paper is to present a general
analysis of the reliability of power spectra and frequency-response
estimates obtained by random-process techniques, particularly as these
are affected by noises. These results have general application to gust
response problems as well as other aeronautical problems. They are also
specifically applied to the interpretation of the results obtained in
the analysis of the present test data.

The present paper is presented in two parts. In the first part
random-process techniques are applied to the flight-test data in order
to determine the various power spectra and frequency-response functions.
The second part is devoted to the reliability of the techniques and pre-
sents a general analysis of the effects of various types of noises on
the measured power spectra and the frequency-response functions. The
results obtained are applied to the flight-test data to assess the reli-
ability of the power spectra and the frequency-response functions obtained.

SYMBOLS

a_n normal acceleration, g units or ft/sec^2

b   airplane span, ft

c( )   co-power spectrum

$\bar{c}$ mean aerodynamic chord

E_1 percent sampling error in amplitude of frequency-response
function

E_2 sampling error in phase of frequency-response function

EI   bending stiffness

f   frequency, cps

$F(\omega)$ frequency-response function of prewhitening operation

g acceleration due to gravity

GJ torsional stiffness

$H(\ )$ frequency-response function

$H_c(\ )$ estimate of frequency-response function obtained by cross-spectrum method

$H_s(\ )$ estimate of frequency-response function obtained by spectrum method

$\left.\begin{array}{l} h,i,k,m, \\ n,p,q \end{array}\right\}$ indices

l distance from center of gravity of airplane to angle-of-attack vane, ft

L scale of turbulence, ft

m number of lags used in calculations for auto- or cross-correlation function

n number of observations in sample of time series

$n(t)$ noise signal

$q(\omega)$ quadrature spectrum

$R_x(\tau)$ auto-correlation function

$R_{xz}(\tau)$ cross-correlation function

R_p designates sum of lagged products used to estimate auto- or cross-correlation function

$R[\ ]$ designates real part of term in brackets

t time, sec

T specified time, sec

Δt time increment between successive readings of time history, sec

V airspeed, ft/sec

w_a airplane vertical velocity, ft/sec

w_g, w   vertical gust velocity, ft/sec

w(t,y)   gust velocity field experienced by airplane as a function of time and airplane span position

x   arbitrary input disturbance

z   arbitrary response

α_v vane-indicated angle of attack, radians

$\gamma^2(\ )$ coherency function

$\Gamma_1(\ ), \Gamma_2(\ )$ span attenuation factors

δ trace deflection

ϵ strain indication, in./in.

ϵ_0 strain indication per g as measured in slow pull-ups

$\epsilon_a = 32.2 \dfrac{\epsilon}{\epsilon_0}$

θ pitch angle, radians

$\dot{\theta}$ pitch velocity, radians/sec

ψ phase angle by which response lags input disturbance

Φ_x power spectral density function

Φ_{xz} cross-spectrum density function

σ root-mean-square deviation

σ_e root-mean-square reading error

τ time lag, sec

ω frequency, radians/sec

Subscripts:

c   calculated by cross-spectrum method

s   calculated by spectrum method

0   initial value at time 0

F   front spar

R   rear spar

    A bar over a symbol denotes a mean value. Prewhitened data is indicated by ^ over a symbol. The complex conjugate is indicated by an asterisk and a quantity contaminated by noise is indicated by a primed symbol. The absolute value of a complex quantity is indicated by | |.

I. DETERMINATION OF FREQUENCY-RESPONSE FUNCTIONS FOR

STRAIN RESPONSE TO VERTICAL GUSTS

AIRPLANE, INSTRUMENTATION, AND TESTS

    The airplane used in the investigation was a B-47A six-engine jet bomber. For the present tests, an airspeed measuring boom, a fairing on the fuselage nose, and an external canopy mounted atop the fuselage to house an optigraph were added to the airplane. A photograph of the airplane is shown in figure 1, and a three-view drawing of the airplane is given in figure 2. The instrumentation pertinent to this report is shown in figure 2. The locations of the strain gages are indicated in inches from the airplane center line as measured perpendicular to the airstream. Some of the airplane characteristics pertinent to the present investigation are given in table I. The estimated wing and fuselage weight distributions applicable to the tests are shown in figure 3. All the fuel load is carried in three main and two auxiliary tanks located within the fuselage. The estimated spanwise torsional and bending stiffness distributions are given in figure 4.

    The instrumentation included an NACA air-damped recording accelerometer mounted near the center of gravity to measure normal acceleration. Electrical wire-resistance strain gages were installed on the front and rear spars at five spanwise locations (fig. 2) in order to obtain a measure of the local wing shear and bending strains. The strain gages were not calibrated against known loads, and the strain-gage outputs are used herein only as local strain indications. The strain-gage outputs were recorded on multichannel oscillographs. A standard NACA pitch-attitude

recorder and a magnetically damped NACA turnmeter were installed near
the center of gravity in order to record the pitch angle and pitching
velocity, respectively. A mass-balanced metal flow vane was mounted on
the nose boom to measure the angle of attack of the airplane for use in
determining the gust velocities.

Additional instrumentation included a standard NACA airspeed-altitude
recorder, a stagnation temperature recorder, and a statoscope. The stato-
scope, which is a sensitive pressure altimeter, was used, as will be dis-
cussed later, to check the vertical velocity of the airplane obtained by
integrating the acceleration record. Control-position recorders were used
to measure the aileron, rudder, and elevator displacements. The control-
position records were used to monitor the flight records in order to
insure that control movements by the pilot did not significantly affect
the flight measurements during the test flights in rough air. A
16-millimeter motion-picture camera was used to photograph the fuel
gages at 2-second intervals, and these recordings were used in deter-
mining the weight of the airplane during the flight tests. A 0.1-second
chronometric timer was used to synchronize all the records. The natural
frequencies, damping, sensitivities, and film speeds of the various
instruments and recorders are given in table II.

The data were obtained during level flight in clear air turbulence
at two altitudes (approximately 5,000 feet and 35,000 feet). The length
of the record samples, the Mach number, weight, and center-of-gravity
position for the two test runs are summarized in the following table:

Altitude, ft	Length of record sample, min	Mach number	Weight, lb	Center-of-gravity position, percent $\bar{c}$
5,000	4.0	0.63	113,000	20.0
35,000	1.5	.64	112,000	20.3

The test weights are low weight conditions for the airplane and do not
represent as severe a gust load condition as a heavier weight. The
piloting techniques used involved slow control movements to correct for
major deviations from the prescribed altitude and heading; minor devia-
tions were not corrected for by the pilot. This control procedure
approximates an elevator-fixed condition inasmuch as the power-boost
control system used on the test airplane causes the control surfaces
to be essentially fixed except for pilot-controlled inputs.

METHODS OF DETERMINING FREQUENCY-RESPONSE FUNCTIONS

One of the basic aims in the present analysis of the data was to derive estimates of the airplane strain response characteristics in rough air as defined by the frequency-response functions. Two methods are known for the determination of the airplane frequency-response functions from measurements of the responses to random and continuous disturbances. These two methods will be referred to as the spectrum and the cross-spectrum methods. In the present investigation, both methods are used. The spectrum and cross-spectrum methods are briefly outlined and the main features of each method are indicated in the following paragraphs.

The spectrum method for the determination of frequency-response functions is based upon the relation between the power spectrum of the response $\Phi_z(\omega)$ of a linear system and of the disturbance $\Phi_x(\omega)$. (See ref. 9.) From this relation, the amplitude squared of the frequency-response function is given by

$$\left| H_s(\omega) \right|^2 = \frac{\Phi_z(\omega)}{\Phi_x(\omega)} \tag{1}$$

where

$\left| H_s(\omega) \right|^2$ amplitude squared of frequency-response function determined by spectrum method

$\Phi_z(\omega)$ power spectrum of airplane response

$\Phi_x(\omega)$ power spectrum of disturbance or gust input

The application of this method simply requires the determination of the power spectrum of the response $\Phi_z(\omega)$ and the power spectrum of the gust input $\Phi_x(\omega)$. One obvious limitation of the spectrum method is that no information on the phase relationship between the input and output responses is obtained. Phase information is frequently required in studies involving multiple disturbances and is also required for the determination of responses to arbitrary disturbances.

The cross-spectrum method is based upon the relationship for linear systems between the power spectrum $\Phi_x(\omega)$ of a random input disturbance and the cross-spectrum $\Phi_{xz}(\omega)$ between the input disturbance and the system response to the disturbance (ref. 9). From this relationship,

the frequency-response function is given by the following expression:

$$H_c(\omega) = \frac{\Phi_{xz}(\omega)}{\Phi_x(\omega)} \tag{2}$$

where

$\Phi_{xz}(\omega)$ cross spectrum between disturbance input and airplane response

$H_c(\omega)$ frequency-response function determined by cross-spectrum method

Both the amplitude and the phase of the frequency-response function $H_c(\omega)$ are obtained since Φ_{xz} is, in general, complex.

The spectrum and cross-spectrum methods should yield identical results for the amplitudes of the frequency-response functions if very long period measurements are available and no extraneous noises are present in the measurements. In most practical applications, the available measurements will be limited and significant noise sources will be present. These two factors can seriously affect the reliability of the results obtained with both methods, each to different extents. In the present applications, noise arises from several sources, such as instrument inaccuracies, reading errors, the effects of other turbulence components on the airplane responses, and the effects of spanwise variations in the turbulence. The errors introduced by these types of noises appear to be large enough to warrant detailed consideration. The second part of this paper is, in fact, devoted to these problems and presents an analysis of the errors arising from these sources.

EVALUATION OF DATA AND RESULTS

The data-reduction procedures used involved the following steps:

(a) Evaluation of the time histories of the pertinent measurements. (The measurements included the bending and shear strains at the various stations, related measurements of airplane acceleration, as well as the quantities required for the determination of the time history of vertical gust velocity.)

(b) Evaluation of the power spectra and cross-spectra for the various quantities.

(c) Determination of the frequency-response functions.

The procedures used in each of these steps will be discussed in order.

Evaluation of Time Histories

Strains.- As an indication of the general characteristics of the records obtained during flight in rough air, short sections of the time histories of the wing bending strains, shear strains, and acceleration at the center of gravity for the low-altitude tests are shown in figure 5. For comparison with these responses, the time history of vertical gust velocity is also shown in the figure; the method used in determining this time history is discussed in detail subsequently.

Evaluation of the strain records consisted of reading the deflection of each of the strain time histories at 0.05-second intervals. This choice was based on sampling considerations as discussed in reference 9 and on the fact that the records indicate little power at frequencies above 10 cycles per second. The deflections read from the strain time histories were processed on automatic digital computers to obtain the incremental strain indication from the relation:

$$\epsilon = \frac{\delta - \bar{\delta}}{\delta_c} \qquad (3)$$

where

ϵ incremental strain indication

δ trace deflection from reference, in.

$\bar{\delta}$ mean trace deflection from reference, in.

δ_c trace deflection from reference due to known voltage (used to compensate for minor voltage fluctuations between the various gages)

Quasi-static reference condition.- In order to obtain a measure of the effects of structural flexibility on the strains at the various stations, a set of quasi-static reference strain histories is desirable for comparison with the actual measured strains. Unfortunately, airplane flight tests cannot provide any direct basis for obtaining such static strains. An indirect method of establishing a set of quasi-static reference strains from the flight-test data which has frequently been found useful in previous studies (for example, refs. 5 and 6) is used in the

present analysis. This method involves two steps: (a) determination
of the aerodynamic loads applied to the airplane, and (b) conversion of
these loads to strains for a quasi-static airplane. For step (a), use
is made of the airplane center-of-gravity accelerations. In reference 6,
it was indicated that for this airplane the airplane acceleration (as
determined by averaging the local accelerations over the airplane mass)
can be closely approximated if the effects of the vibrations associated
with the higher frequencies (above 2 cps) are removed from the center-
of-gravity acceleration measurements. This objective was accomplished
by a visual fairing of the record and is roughly equivalent to the appli-
cation of a low-pass filter with a cutoff at about 2 cps. This faired
center-of-gravity acceleration was then used to provide a direct measure
of the airplane loading. For step (b), these loads were converted to
strains by using the strains per unit load (per g) as measured in slow
pull-up maneuvers at the same speed and altitude. The values of strains
per g used were reported in references 6 and 7 and are given in table III.
(This procedure essentially neglects the interaction between the dynamic
airplane vibrations and the aerodynamic forces and assumes that the span
load distribution and the wing and tail contributions in gusts are the
same as in pull-ups.) The strain measurements obtained on this basis may
be viewed as an approximation to the strains that would be obtained for
a pseudo-static airplane, that is, an airplane restrained from dynamic
vibration. Consequently, comparison of the strains obtained on this
basis with the measured strains in rough air provides a measure of the
effects of airplane dynamic flexibility.

   Normalization procedure.- In order to facilitate comparisons between
the strain measurements at the various stations and the strain for the
quasi-static reference condition, all strain measurements were normalized
by using the strain values per unit load as measured in pull-ups for the
various stations. The normalized measurements are defined as follows:

$$\epsilon_a = 32.2 \frac{\epsilon}{\epsilon_0} \tag{4}$$

where ϵ_0 is the strain indication per g as measured at the various sta-
tions in slow pull-ups at the same speed and dynamic pressure. The nor-
malized values of strain indication ϵ_a may thus be viewed as having the
same units as acceleration, that is, feet per second per second. The
results for the various power spectra and frequency-response functions
of the strain measurements will be presented in this form. This form of
presentation has the special merit of permitting the use of a single
quasi-static reference strain spectrum or frequency-response function for
direct comparison with the strain responses at the various stations; it
thus also permits direct comparison of the relative effects of flexibility
on the strains for the various stations.

Vertical-gust velocity.- The method used to determine the vertical-gust velocity is essentially that given in reference 10 and is based on flow-direction vane measurements and involves corrections for airplane motions. The method of reference 10 relates the vertical-gust velocity to the vane-indicated angle of attack and airplane motions by the following equation:

$$w_g = V\alpha_v - V\theta + w_a + l\dot{\theta} \tag{5}$$

where

w_g vertical-gust velocity, ft/sec

V airplane forward speed, ft/sec

α_v vane-indicated angle of attack, radians

θ pitch angle, radians

w_a airplane vertical velocity, ft/sec (The sign convention of w_a is positive upward and is opposite to that used in ref. 10)

$\dot{\theta}$ pitching velocity, radians/sec

l distance from angle-of-attack vane to center of gravity of airplane, ft

Equation (5) is based on the following assumptions:

(1) All disturbances are small.

(2) Bending of the boom which supports the vane is negligible.

(3) The effects of variations in upwash on the vane-indicated angle of attack are negligible.

In the application of equation (5), a number of problems are encountered. The pitch-attitude measurements, as is frequently the case, contained a slow rate of drift. It was therefore decided to determine θ by integration of measurements of pitch velocity $\dot{\theta}$. In addition, w_a was not measured directly but was determined by integration of the center-of-gravity normal acceleration measurements. All measurements were read as increments from the mean values for the whole record. With these modifications, the actual evaluation procedures are given by:

$$w_g = V\left(\alpha_V - \bar{\alpha}_V\right) - V \int_0^t \left(\dot{\theta} - \bar{\dot{\theta}}\right)dt - V\theta_0 + \int_0^t \left(a_n - \bar{a}_n\right)dt +$$

$$w_0 + l\left(\dot{\theta} - \bar{\dot{\theta}}\right) \tag{6}$$

Values of the pitching velocity $\dot{\theta}$ and the acceleration a_n were read at 0.05-second intervals and the vane-indicated angle of attack α_V at 0.1-second intervals. The quantities $\dot{\theta} - \bar{\dot{\theta}}$ and $a_n - \bar{a}_n$ were then numerically integrated by use of the trapezoidal rule. (As discussed in ref. 11, this method of integration attenuates the higher frequencies; the amount of attenuation in the integrated results increases with increasing frequency. In the present case, where the integrations were performed by using 0.05-second-interval readings, the attenuation is negligible at the lower frequencies, about 5 percent at a frequency of 2.5 cps, and 20 percent at a frequency of 5 cps.) The initial value of the vertical velocity of the airplane w_0 was estimated from the slope of the pressure altitude record taken with the statoscope. As a check on the integrations, the acceleration $a_n(t)$ was integrated twice and compared with the altitude trace taken with the statoscope. The initial incremental value of the pitch angle θ_0 could not be accurately determined and the term was therefore omitted in the computations. This omission has a negligible effect on the calculated power spectra of the gust velocity.

The time history of the vertical-gust velocity for the 4-minute test flight at 5,000 feet was determined at time intervals of 0.1 second. For the high-altitude tests, large-amplitude high-frequency oscillations of the vane-indicated angle of attack were present. The poor quality of the vane record for these high-altitude tests is apparently the result of the decrease in aerodynamic damping of the vane at high altitude. Reliable gust-velocity measurements could not be obtained for these data and thus no use will be made of the gust data for the high-altitude run. As a consequence, frequency-response functions could not be determined for this case.

Power Spectra and Cross-Spectra Determinations

Power spectra.- The procedures used in the determination of the power spectra and cross-spectra are essentially the same as those outlined in reference 9. The power spectrum of a disturbance $x(t)$ is defined by

$$\Phi_x(\omega) = \frac{2}{\pi} \int_0^\infty R_x(\tau) \cos \omega\tau \, d\tau \qquad (7)$$

where $R_x(\tau)$ is the autocorrelation function defined by

$$R_x(\tau) = \lim_{T \to \infty} \frac{1}{T} \int_{-T/2}^{T/2} x(t)\, x(t+\tau)\, dt \qquad (8)$$

The numerical procedures used for n equally spaced readings $x_1, \ldots x_n$ involve the estimation of values of $R_x(\tau)$ for $m + 1$ evenly spaced values of τ from 0 to $m \, \Delta t$ by

$$R_p = \frac{1}{n - p} \sum_{q=1}^{n-p} x_q x_{q+p} \qquad (p = 0, 1, \ldots m) \quad (9)$$

First raw estimates of the power are obtained by

$$L_h = \frac{2 \, \Delta t}{\pi} \sum_{p=0}^{m} a_p R_p \cos \frac{hp\pi}{m} \qquad (h = 0, \ldots m) \quad (10)$$

where

$$a_p = 1 \qquad\qquad (0 < p < m)$$

$$a_p = \frac{1}{2} \qquad\qquad (p = 0, m)$$

Final or smoothed estimates of the power are then obtained by

$$\left. \begin{aligned} \Phi_0 &= \frac{1}{2} L_0 + \frac{1}{2} L_1 \\[2mm] \Phi_h &= \frac{1}{4} L_{h-1} + \frac{1}{2} L_h + \frac{1}{4} L_{h+1} \qquad (1 < h < m - 1) \\[2mm] \Phi_m &= \frac{1}{2} L_{m-1} + \frac{1}{2} L_m \end{aligned} \right\} \qquad (11)$$

As discussed in reference 9, these estimates are averages of the power over the frequency range $\dfrac{h\pi}{m\,\Delta t} \pm \dfrac{2\pi}{m\,\Delta t}$.

In the actual reduction of the data, the time-history data for the low-altitude tests were first divided into two segments, designated hereafter as samples 1 and 2 and covering the first and second 2 minutes of flight in rough air, respectively, in order to have a check on the consistency of the results. Power spectra were then obtained of the measured accelerations a_n and the incremental strain indications ϵ_a for both samples 1 and 2 of the low-altitude data. For the high-altitude data, no such division was used owing to the short sample available. The power spectra were determined from 0.05-second-interval readings ($\Delta t = 0.05$) and for a value of $m = 60$. The calculations thus yielded 61 power estimates uniformly spaced over the frequency range of 0 to 10 cps. This frequency range appears to be sufficient to cover all the predominant frequencies present in the various responses.

As an illustration of the consistency of the data, the power spectra of a_n for samples 1 and 2 of the low-altitude tests are plotted in figure 6. The root-mean-square values of acceleration σ are also shown in figure 6. Except for a difference in intensity, the two spectra are very similar. A comparison of the power spectra of a_n for the tests at 5,000 feet and 35,000 feet altitude is given in figure 7.

The power spectra of the strains ϵ_a for the front and rear spars at various spanwise stations and at the two altitudes are given in figures 8 and 9 for the bending and shear strains, respectively. (The results $\Phi(f)$ presented in figures 8 and 9 are in terms of the frequency argument f, where $\Phi(f) = 2\pi\Phi(\omega)$.) The strain spectra shown are for sample 1 inasmuch as the differences between the spectra for the two samples were, in all cases, small and similar to the difference between the power spectra of a_n for samples 1 and 2 shown in figure 6. In each case, the power spectrum of the airplane acceleration (faired center-of-gravity acceleration) is shown as the quasi-static reference.

Prewhitening of vertical-gust velocity.- Inasmuch as the power spectra of gust velocity were expected to have a large peak in power at the low frequencies (based on examination of the gust time history and previously obtained gust spectra), the gust time history was filtered or prewhitened (see ref. 9) to minimize the possible distortion of the power spectra from diffusion of power from the low frequency end to the high frequencies. In order to reduce the relative power at the low frequencies, a high pass digital filter was applied to the time history data of vertical-gust velocity w_g. The filter used is defined by

$$\hat{w}_g(t) = w_g(t) - w_g(t-\Delta t) \qquad (12)$$

where

$\hat{w}_g$ prewhitened gust velocity

Δt time interval between successive values of w_g (0.1 second for present application)

This linear operation in the time plane corresponds to the multiplication in the frequency plane by the function

$$F(\omega) = 1 - e^{-i\omega\Delta t} \qquad (13)$$

Thus, the Fourier transforms of $\hat{w}_g(t)$ and $w_g(t)$ $\left(\text{denoted by } \hat{W}_g(\omega) \text{ and } W_g(\omega)\right)$ are related by

$$\hat{W}_g(\omega) = \left(1 - e^{-i\omega\Delta t}\right)W_g(\omega) \qquad (14)$$

The operation involves both an amplification and phase shift. The relation between the power spectra of $w(t)$ and $\hat{w}(t)$ is then given by

$$\left. \begin{aligned} \Phi_w(\omega) &= \frac{\Phi_{\hat{w}}(\omega)}{|F(\omega)|^2} \\[2em] \Phi_w(\omega) &= \frac{\Phi_{\hat{w}}(\omega)}{2 - 2\cos\omega\,\Delta t} \end{aligned} \right\} \qquad (15)$$

and must be applied to the power spectrum of $\Phi_{\hat{w}}(\omega)$ in order to recover the desired spectrum $\Phi_w(\omega)$.

The power spectra of vertical gust velocity for the two parts of the low-altitude test run are shown in figure 10 as a further check on the consistency of the results.

Cross-spectra.- The cross-spectra between the vertical-gust velocity and the various airplane responses were also determined by using the general procedures outlined in reference 9. The cross-spectrum between a disturbance $x(t)$ and a response $z(t)$ is defined by

$$\left. \begin{array}{l} \Phi_{xz}(\omega) = \dfrac{1}{\pi} \displaystyle\int_{-\infty}^{\infty} R_{xz}(\tau)e^{-i\omega\tau}d\tau \\[3em] \Phi_{xz}(\omega) = c(\omega) - iq(\omega) \end{array} \right\} \qquad (16)$$

where $R_{xz}(\tau)$ is the cross-correlation function; $c(\omega)$ is the cospectrum; and $q(\omega)$ is the quadrature spectrum. These terms are defined by

$$R_{xz}(\tau) = \lim_{T \to \infty} \frac{1}{T} \int_{-T/2}^{T/2} x(t) \, z(t+\tau) \, dt \qquad (17)$$

$$c(\omega) = \frac{2}{\pi} \int_{0}^{\infty} \frac{R_{xz}(\tau) + R_{xz}(-\tau)}{2} \cos \omega\tau \, d\tau \qquad (18)$$

$$q(\omega) = \frac{2}{\pi} \int_{0}^{\infty} \frac{R_{xz}(\tau) - R_{xz}(-\tau)}{2} \sin \omega\tau \, d\tau \qquad (19)$$

The numerical procedures used involved the determination of $R_{xz}(\tau)$ at equally spaced values of τ from the n equally spaced readings $x_1, \ldots x_n$ and $z_1, \ldots z_n$ by the relation

$$R_p = \frac{1}{n-p} \sum_{q=1}^{n-p} x_q z_{q+p} \qquad (p = -m, \ -(m-1), \ \ldots \ m) \qquad (20)$$

Cospectrum and quadrature spectrum estimates are then obtained by

$$c_h = \frac{\Delta t}{\pi} \sum_{p=0}^{m} a_p \left(R_p + R_{-p} \right) \cos \frac{hp\pi}{m} \qquad (h = 0, \ 1, \ \ldots \ m) \qquad (21)$$

$$q_h = \frac{\Delta t}{\pi} \sum_{p=0}^{m} a_p \left(R_p - R_{-p} \right) \sin \frac{hp\pi}{m} \qquad (h = 0, \ 1, \ \ldots \ m) \qquad (22)$$

where

$$a_p = \frac{1}{2} \qquad (p = 0, m)$$

$$a_p = 1 \qquad (p \neq 0, m)$$

The smoothing operation given by equation (11) for the spectra is also applied to the cross-spectrum estimates. The final estimates also provide estimates of the average power over the frequency range $\dfrac{h\pi}{m \Delta t} \pm \dfrac{2\pi}{m \Delta t}$.

In the application of these relations to the present data, the prewhitened time history of the gust velocity was used. The compensation for this prewhitening thus requires that estimates of the cross-spectrum be divided by $F(-\omega)$ (from eq. (13)) in order to obtain the appropriate results. Thus, the desired cross-spectrum $\Phi_{xy}(\omega)$ is obtained from the cross-spectrum $\Phi_{\hat{x}z}(\omega)$ based on the prewhitened gust time history by the relation

$$\Phi_{xz}(\omega) = \frac{\Phi_{\hat{x}z}(\omega)}{1 - e^{i\omega\Delta t}} \tag{23}$$

Frequency-Response Functions

The results obtained from the foregoing procedures for the required power spectra and cross-spectra may be used in equations (1) and (2) to obtain estimates of the frequency-response functions. In terms of the quantities defined in equations (11), (21), and (22), these relations become

$$\left| H_s(\omega) \right|^2 = \frac{(\Phi_z)_h}{(\Phi_x)_h} \tag{24}$$

and

$$\left| H_c(\omega) \right| = \frac{\left(c_h{}^2 + q_h{}^2 \right)^{1/2}}{(\Phi_x)_h} \tag{25}$$

the phase lag $\psi(\omega)$ of the response being given by

$$\psi(\omega) = \tan^{-1} \frac{q_h}{c_h} \qquad \qquad (26)$$

where $\omega = \frac{h\pi}{m \, \Delta t}$ and $h = 0, 1, \ldots m$. These estimates are, of course, for the average over the respective band widths as was the case for the individual power spectra and cross-spectra.

Frequency-response functions of the center-of-gravity acceleration and of, the wing strains at the different stations were calculated by both the spectrum and cross-spectrum methods for the low-altitude tests. As an illustration of the difference between the frequency-response functions obtained by the two methods, the two frequency-response functions for the center-of-gravity acceleration are given in figure 11(a). The reasons for the observed differences are explored in the second part of this paper and will be discussed in detail therein.

In general, the analysis of the second part of this paper indicates that the cross-spectrum estimates are less subject to systematic errors or distortions arising from a variety of noise sources. In addition, only the cross-spectrum methods provide phase information. For these reasons, only the results obtained by the cross-spectrum methods are presented. Figures 12 and 13 present the frequency-response functions obtained for the bending and shear strain responses at the various stations. These results form the principal results of the present investigation. The frequency-response function for the faired center-of-gravity acceleration, which, as indicated earlier, is used to represent a reference quasi-static airplane condition, is also given in each case for comparison.

Inasmuch as the gust velocity was only determined at time increments Δt of 0.1 second, the cross-spectra and frequency-response functions were based on the 0.1-second time interval readings and 61 estimates ($m = 60$) were obtained for the frequency region of 0 to 5 cycles per second. As a consequence, there is some distortion arising from power present above 5 cycles per second due to "foldover" effects. (See ref. 9.) These distortions are, however, generally negligible below 2 cycles per second and are small between 2 to 3 cycles per second. Also, the analysis of part II indicates that the results at the higher frequencies, above 3 cycles per second, are too unreliable for use. Accordingly, the results shown in figures 12 and 13 are restricted to the frequency region of 0 to 3 cps. For this frequency region, the present results tend to underestimate the true values by an amount that increases with frequency from about 5 percent at 0.3 cps to values in excess of 30 percent above 2 cps.

The frequency-response functions shown in figures 12 and 13 are based only on calculations for sample 1 in order to reduce the calculation

burden. In a few cases, the frequency-response functions were also determined for sample 2 in order to check the consistency of the results. Figure 14 shows a comparison of the results obtained for the two samples by the cross-spectrum method for the case of the normal acceleration response. The results are seen to be in good agreement, as might be expected from the sampling theory considerations of part II. Equivalent consistent results were also obtained for several of the strain responses and thus this reduction in calculation time was justified.

EFFECTS OF AIRPLANE FLEXIBILITY ON WING STRUCTURAL STRAINS

Power Spectra of Strains

Examination of the power spectra of bending strains (fig. 8) for the low-altitude tests indicates that almost all the strain power is concentrated at frequencies below about 2 cps for both the front and rear spars. In this frequency region, the power appears to be concentrated in three principal lobes or peaks: a power peak close to zero frequency, a second peak at 0.5 cps, and a third large peak at 1.5 cps. The very low frequency power peak is largely confined to the outboard stations and appears to be a reflection of the airplane rolling response to side gusts, aileron control motions, and asymmetries across the airplane span in the vertical gusts. This peak thus has no relation to airplane flexibility effects. The second power peak at 0.5 cps is associated with the airplane short-period mode and is of relatively uniform magnitude at the several stations. The small variations in the magnitude of this peak are, to a large degree, probably associated with minor inaccuracies in the strain per g values of table III obtained from the pull-up maneuvers. The power peak at 1.5 cps is a reflection of the airplane first bending mode. At the inboard station, this peak is not as pronounced as is the short-period power peak. However, at the midspan stations, the magnitude of this first bending peak increases by a large amount and provides the major contribution to the strains at these stations.

Comparison of the power spectra of the strains at the various stations with the reference power spectrum indicates that the effects of flexibility are principally reflected in large amplifications of the strain responses in the frequency region of the fundamental wing-bending mode. At frequencies above 2 cps, there is some reflection of the effects of higher structural modes, particularly at the outboard stations where a moderate power peak at 4.5 cps can be discerned. There appears to be little difference between the power spectra of bending strain for the front and rear spar.

In order to obtain a simple overall measure of the effects of dynamic flexibility on the strains, the root-mean-square values for the various power spectra were determined and are shown in figure 8. For this purpose, the power in the peaks of the spectra for the outboard stations at

very low frequency (below 0.3 cps) was not used inasmuch as this power
appears to be associated with the airplane lateral response motions and
has no bearing on elastic response characteristics. The root-mean-square
values are seen to be lowest for the root station and increase to about
twice this value for the midspan station. Comparing these values with
the root-mean-square values for the reference condition indicates that
the overall amplification in root-mean-square strain arising from elastic
effects is about 10 percent at the root and increases to about 100 per-
cent at the midspan stations.

The power spectra for the strains for the high altitudes (fig. 8(b))
show much the same general characteristics as those observed for the
low-altitude data. Two observations are worth noting for the high-
altitude data: first, the indication that the peak in strain power
associated with the first bending mode at a frequency of 1.5 is much
more pronounced in this case than in the case of the low-altitude data.
This condition indicates that the dynamic amplification associated with
flexibility is more pronounced at the higher altitudes as a consequence
of the lower aerodynamic damping associated with the reduced dynamic
pressure. A second point of interest is the clear reflection of a sharp
peak in the quasi-static reference power spectrum. This peak is a
reflection of the increased effect of the first flexible mode on the
center-of-gravity accelerations at the high altitudes. As a consequence,
this spectrum is not as well suited for a quasi-static reference condi-
tion for determining dynamic amplifications as was the case for the low-
altitude tests.

The root-mean-square strain values for the various spectra are also
shown for the high-altitude results. Comparing the values for the vari-
ous stations with the root-mean-square value for the quasi-static refer-
ence condition indicates that the overall strain amplification arising
from structural dynamics is about 20 percent at the root station and
increases to about 100 percent at the midspan station.

The power spectra of the shear strains of figure 9 show much the
same general characteristics as the bending strains. A number of dif-
ferences are, however, worth noting. First, the effects of the rolling
motions on the strain peak close to zero frequency seem more pronounced
in the case of shear strains than was the case for the bending strains.
In addition, the effects of the higher structural modes are also more
evident with indications of minor strain peaks at frequencies of 2.2,
3.2, and 4.5 cps. Comparison of the strain records obtained at the
inboard stations on the right and left wings indicates that the struc-
tural modes at 2.2 and 4.5 cps are antisymmetric modes. A final point
worth noting for the shear strain responses is the large variations
between the power spectra for the front and rear spars at the various
stations. The overall effects of flexibility on the shear strains as
reflected by the root-mean-square strains appear to follow the same
general pattern noted for the bending strains but display somewhat

larger strain amplifications and a somewhat less orderly pattern. The lower value for the root station than for the reference condition is somewhat unexpected and is believed to be in part a result of minor inaccuracies in the strain per g values determined from the pull-up data.

Frequency-Response Functions

The frequency-response functions of figures 12 and 13 serve to indicate in a clearer fashion the overall effects of the flexibility. Consideration of the results presented in these figures indicates that the effects of flexibility show up principally in a large amplification of strains in the neighborhood of the first bending mode. As one considers the various frequency-response functions from the root station to the outboard stations, it is clear that the peak associated with the first flexible mode is small at the root station but increases rapidly toward the midspan stations. The effects of the first flexible mode appear to be relatively small at the farthest outboard station. When the results obtained for the phase are considered, it appears that at low frequencies the strain responses are essentially in phase with the airplane acceleration response. However, at frequencies above 1 cps, the strain response lags the acceleration response by an increasing amount as the frequency increases. Above 2 cps the phase data are somewhat erratic. This behavior is believed to be in part the effect of the complicated phase behavior at these frequencies and the limited reliability of the results at the higher frequencies.

It should be noted that the amplitudes of the frequency-response functions given in figures 12 and 13 are, to some degree, contaminated by systematic errors or distortions resulting from the presence of noise in the measurements. The analysis given in part II indicates the amplitudes are too low by an amount that varies with frequency, increase slowly from 0 percent at 0 cps to 5 percent at 0.3 cps, and then increase more rapidly to about 30 percent at 2 cps and 50 percent at 3 cps. Adjustments for these distortions should be made when the present results are compared with results obtained in other investigations for this airplane. These adjustments should also, of course, be used in the calculations of the responses of the present airplane to other gust disturbances.

II. RELIABILITY OF ESTIMATES OF FREQUENCY-RESPONSE

FUNCTIONS OBTAINED BY RANDOM-PROCESS TECHNIQUES

In part I of the present paper, it was indicated that the frequency-response function $H(\omega)$ of a linear system can be estimated from measurements of the response $z(t)$ of the system to a random-input disturbance $x(t)$. For this case, estimates of the frequency-response function for the response $z(t)$ to unit sinusoidal disturbances in $x(t)$ may be determined by either the spectrum method or the cross-spectrum method as given by the following expressions:

$$\left|H_{B}(\omega)\right|^{2} = \frac{\Phi_{z}(\omega)}{\Phi_{x}(\omega)} \tag{27}$$

and

$$H_{c}(\omega) = \frac{\Phi_{xz}(\omega)}{\Phi_{x}(\omega)} \tag{28}$$

where

$\Phi_{x}(\omega), \Phi_{z}(\omega)$ power spectra of $x(t)$ and $z(t)$, respectively

$\Phi_{xz}(\omega)$ cross-spectrum between $x(t)$ and $z(t)$

Note that only the amplitude of the frequency-response function may be obtained from the spectrum method (eq. (27)) whereas both the amplitude and phase of the frequency-response function are obtained from the cross-spectrum method (eq. (28)). In many applications of these methods, such as those given in this paper, the reliability of the spectra and the frequency-response function estimates appears to depend heavily upon the extent to which extraneous disturbance factors, which might be termed noise, are present in the measurements. The purpose of this section is to examine the manner in which the estimates obtained by these two methods are affected by various types of noises. The types of noises to be considered include: (a) random errors in $x(t)$ and $z(t)$ that might be introduced by instrument and reading error, (b) effects of extraneous disturbances such as other turbulence components on the response $z(t)$, and (c) effects of spanwise variations in the turbulence. In general, noises of these types have two principal effects on the estimates. First, noises introduce systematic errors or distortions in the estimates, and second, noises give rise to a decrease in the statistical reliability or an increase in random sampling errors. The effects of the various types of noises on these two types of errors are first established in a general form. These results are then used to establish the reliability of the estimates of the frequency-response functions obtained from the test data.

COHERENCY FUNCTION AND STATISTICAL RELIABILITY

Coherency Function

In the analysis of the relations between any two random processes $x(t)$ and $z(t)$, such as the input gust disturbances and the strain

responses of the present study, the concept of a coherency function $\gamma^2(\omega)$ as defined by

$$\gamma^2(\omega) = \frac{\left|\Phi_{xz}(\omega)\right|^2}{\Phi_x(\omega)\ \Phi_z(\omega)} \tag{29}$$

is known to play a central role. (See ref. 12.) The coherency function may be viewed as a measure of the degree to which two processes are linearly related. If two processes are in perfect linear relation, then the coherency function has a value of unity for all frequencies. At the other extreme, if two processes are linearly independent, then the cross-spectrum $\Phi_{xz}(\omega) = 0$ and likewise $\gamma^2(\omega) = 0$. Such uncorrelated processes are termed incoherent. For two processes which are only partially linearly related, as is the case when extraneous noise is present, the coherency function will lie between 0 and 1, the value depending upon the ratio of the coherent power of the two processes to the total power as given by equation (29).

The coherency function can also be expressed in terms of the quantities H_c and H_s and from equations (27) to (29).

$$\gamma^2(\omega) = \frac{\left|H_c(\omega)\right|^2}{\left|H_s(\omega)\right|^2} \tag{30}$$

If the coherency function is equal to one, the estimates of the amplitude obtained by the two methods will be identical. However, if the coherency function is less than one, the estimates of the amplitude of the frequency response based on the spectrum and cross-spectrum differ. Either one or both of the estimates may be distorted, the amount of distortion depending upon the character of the extraneous noise, as will be seen subsequently. Thus, the reduction of the coherency function from the perfect value of unity provides a danger signal that distortions may be present in the estimates. The amount of distortion present, in any given case, depends upon the character of the noise and whether it affects the input or output as will be indicated. The effects of various types of noises are examined in order to establish their effects on the coherency function and to establish the associated distortions.

Statistical Reliability

The coherency function is also important in connection with the magnitude of the sampling errors. In reference 12, the statistical reliability of estimates of the frequency-response function is derived

for the case of stationary Gaussian random processes. The results
obtained therein indicate that the statistical reliability of the esti-
mates obtained for the frequency-response function $\left(H_c(\omega) \text{ or } H_s(\omega)\right)$
depends upon the three basic quantities: the sample size n or number
of readings, the number of frequency points at which estimates are
derived m, and the coherency function $\gamma^2(\omega)$ between the measured
input and the measured response. Figure 15 is based on the results of
reference 12 and gives the 90-percent confidence bands for the quantity

$$\pm E_1 = 100 \frac{|H_c(\omega)| - |H(\omega)|}{|H(\omega)|} \tag{31}$$

which is the percent error in the amplitude of the frequency-response
function and for the quantity E_2, the error in the phase angle. These
quantities permit the establishment of the interval within which the
amplitude and phase angle for the true frequency-response function $H(\omega)$
will probably lie. For example, for $n = 1,000$, $m = 60$, and $\gamma^2 = 0.90$,
the percent error E_1 in the amplitude is ± 15 percent. Thus,

$$-0.15 < \frac{|H_c(\omega)| - |H(\omega)|}{|H(\omega)|} < 0.15 \tag{32}$$

with a probability of 90 percent. It follows from equation (32) that
the associated 90-percent confidence band for the true value of the
amplitude of the frequency-response function $H(\omega)$ is given by

$$0.87 |H_c(\omega)| < |H(\omega)| < 1.17 |H_c(\omega)| \tag{33}$$

The confidence band for the phase angle may also be obtained from fig-
ure 15 and is given by the interval defined by the measured phase angle
plus and minus E_2, the value obtained from figure 15. For $n = 1,000$,
$m = 60$, and $\gamma^2 = 0.90$, $E_2 = \pm 0.15$ radian.

Examination of figure 15 indicates that, for a given sample size n
and a given value of m, the percent error and thus the width of the con-
fidence bands increase rapidly as the coherency decreases. For example,
for $n = 1,000$ and $m = 60$, the percent error in amplitude increases
from about ± 15 percent for $\gamma^2 = 0.90$ to ± 40 percent at $\gamma^2 = 0.50$ and
to ± 70 percent at $\gamma^2 = 0.25$. Similarly, the confidence band for the
phase angle increases from about ± 0.15 radian at $\gamma^2 = 0.90$ to
± 0.75 radian at $\gamma^2 = 0.25$. Thus, the statistical reliability of the
results is strongly dependent upon the level of the coherency function.

## EFFECTS OF NOISES ON FREQUENCY-RESPONSE FUNCTION ESTIMATES

Elementary Cases of Noise

The effects of the presence of noises in the measured quantities, the input $x(t)$ or the response $z(t)$, on the spectra, cross-spectra, coherency functions, and the estimates of the frequency function will be examined in this section of the paper. The basic approach to be used will consist of considering the input and output $x(t)$ and $z(t)$ to be contaminated by a random noise $n(t)$. Thus, the contaminated quantities are given by

$$
\left.
\begin{aligned}
x'(t) &= x(t) + n_1(t) \\
z'(t) &= z(t) + n_2(t)
\end{aligned}
\right\} \tag{34}
$$

where $n_1(t)$ and $n_2(t)$ are used to designate a random noise in the input and output measurements, respectively. The average effect of these noises on the various quantities may be examined by substituting the contaminated quantities of equation (34) for their uncontaminated counterparts in equations (27), (28), and (29).

Two elementary cases of noise contamination and their combination are first considered in this section. These cases are defined by the following sketches:
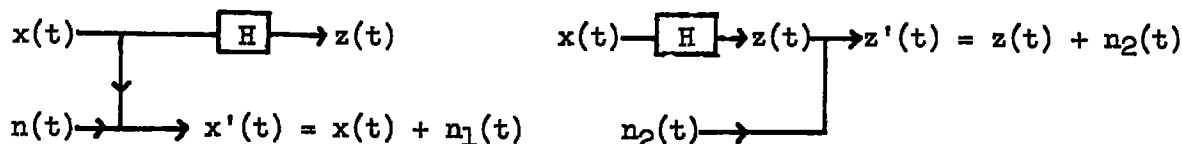
(a) Noise in measured input   (b) Noise in measured output

Case (a): Noise in measured input.- If the input is contaminated by a random noise $n_1(t)$, the following relations exist between the spectra and cross-spectra involving $x(t)$ and $x'(t)$:

$$
\Phi_{x'}(\omega) = \Phi_x(\omega) + \Phi_{n_1}(\omega) + 2R\left[\Phi_{xn_1}(\omega)\right] \tag{35}
$$

and

$$\Phi_{x'z}(\omega) = \Phi_{xz}(\omega) + \Phi_{n_1z}(\omega) \tag{36}$$

where the double subscripts are used to designate the respective cross-spectra and R designates the real part of the complex quantity. Thus, both the input spectrum and the cross-spectrum are contaminated by noise terms. The frequency-response function estimates based on the contaminated input $x'(t)$ will in turn yield

$$\left|H_s(\omega)\right|^2 = \frac{\Phi_z(\omega)}{\Phi_x(\omega) + \Phi_{n_1}(\omega) + 2R\left[\Phi_{xn_1}(\omega)\right]} \tag{37}$$

and

$$H_c(\omega) = \frac{\Phi_{xz}(\omega) + \Phi_{n_1z}(\omega)}{\Phi_x(\omega) + \Phi_{n_1}(\omega) + 2R\left[\Phi_{xn_1}(\omega)\right]} \tag{38}$$

It is clear that in both cases the estimates of the frequency-response function are contaminated by noise terms but the noise affects each estimate in a different manner. In each case, the degree of contamination depends upon the noise level and its relation to the input. For the special case of noise which is incoherent to the input $\left(\Phi_{xn_1}(\omega) = 0\right)$, a simpler result is obtained and this case is of particular interest. For this case, only the input spectrum is contaminated; thus

$$\left|H_s(\omega)\right|^2 = \frac{\Phi_z(\omega)}{\Phi_x(\omega) + \Phi_{n_1}(\omega)} \tag{39}$$

and

$$H_c(\omega) = \frac{\Phi_{xz}(\omega)}{\Phi_x(\omega) + \Phi_{n_1}(\omega)} \tag{40}$$

If $\Phi_{n_1}(\omega) \ll \Phi_x(\omega)$,

$$\left.\begin{array}{l} \left|H_{s}(\omega)\right| \approx \left|H(\omega)\right| \left[1 - \dfrac{\Phi_{n_1}(\omega)}{2\Phi_x(\omega)}\right] \\[20pt] H_c(\omega) \approx H(\omega)\left[1 - \dfrac{\Phi_{n_1}(\omega)}{\Phi_x(\omega)}\right] \end{array}\right\} \tag{41}$$

Thus, the degree of contamination at the various frequencies is proportional to the noise-to-signal ratio in both cases but is twice as large in the cross-spectrum case as in the spectrum case. Both estimates tend to underestimate the amplitude of the frequency-response functions. However, the estimate of the phase obtained by the cross-spectrum method is unaffected since both the real and imaginary terms are contaminated to the same degree.

The coherency function for the general case of noise in the input is given by

$$\gamma^2(\omega) = \frac{\left|\Phi_{xz}(\omega) + \Phi_{n_1 z}(\omega)\right|^2}{\Phi_z(\omega)\left\{\Phi_x(\omega) + \Phi_{n_1}(\omega) + 2R\left[\Phi_{xn_1}(\omega)\right]\right\}} \tag{42}$$

which for the case of incoherent noise reduces to

$$\left.\begin{array}{l} \gamma^2(\omega) = \dfrac{1}{1 + \dfrac{\Phi_{n_1}(\omega)}{\Phi_x(\omega)}} \\[24pt] \gamma^2(\omega) \approx 1 - \dfrac{\Phi_{n_1}(\omega)}{\Phi_x(\omega)} \end{array}\right\} \tag{43}$$

The reduction in $\gamma^2(\omega)$ thus depends directly on the ratio of the noise power to the input signal power.

Note that from equations (39) and (43)

$$\left|H(\omega)\right| = \frac{1}{\gamma^2(\omega)}\left|H_c(\omega)\right| = \frac{1}{\gamma(\omega)}\left|H_s(\omega)\right| \tag{44}$$

Thus, the coherency ratio may be used directly for this case to adjust for the distortions due to random and incoherent input noise.

Case (b): Noise in measured output.- For the case of noise in output, only the spectra involving the output are contaminated and the estimates yield

$$\left.\begin{array}{l}\left|H_s(\omega)\right|^2 = \dfrac{\Phi_z(\omega) + \Phi_{n_2}(\omega) + 2R\left[\Phi_{n_2 z}(\omega)\right]}{\Phi_x(\omega)} \\[4mm] H_c(\omega) = \dfrac{\Phi_{xz}(\omega) + \Phi_{xn_2}(\omega)}{\Phi_x(\omega)}\end{array}\right\} \tag{45}$$

which, for the case of incoherent noise, reduces to

$$\left.\begin{array}{l}\left|H_s(\omega)\right|^2 = \dfrac{\Phi_z(\omega) + \Phi_{n_2}(\omega)}{\Phi_x(\omega)} \\[4mm] \left|H_s(\omega)\right|^2 = \left|H(\omega)\right|^2\left[1 + \dfrac{\Phi_{n_2}(\omega)}{\Phi_z(\omega)}\right]\end{array}\right\} \tag{46}$$

and

$$\left.\begin{array}{l}H_c(\omega) = \dfrac{\Phi_{xz}(\omega)}{\Phi_x(\omega)} \\[4mm] H_c(\omega) = H(\omega)\end{array}\right\} \tag{47}$$

Thus for this case, the cross-spectrum method yields unbiased estimates of both the amplitude and phase of the frequency-response function whereas

the spectrum estimate of the amplitude is distorted and overestimated in proportion to the ratio of noise power to the output signal power.

The coherency for this case $\gamma^2(\omega)$ is given by

$$\gamma^2(\omega) = \frac{\left|\Phi_{xz}(\omega) + \Phi_{xn_2}(\omega)\right|^2}{\Phi_x(\omega)\left\{\Phi_z(\omega) + \Phi_{n_2}(\omega) + 2R\left[\Phi_{n_2z}(\omega)\right]\right\}} \qquad (48)$$

which reduces in the case of a noise which is incoherent to the output to

$$\gamma^2(\omega) = \frac{1}{1 + \dfrac{\Phi_{n_2}(\omega)}{\Phi_z(\omega)}} \qquad (49a)$$

or

$$\gamma^2(\omega) \approx 1 - \frac{\Phi_{n_2}(\omega)}{\Phi_z(\omega)} \qquad \left(\Phi_{n_2}(\omega) \ll \Phi_z(\omega)\right) \quad (49b)$$

where the coherency is reduced by the ratio of noise power to output signal power. In this case, also, uncontaminated estimates may be recovered. Note that in this case,

$$\left.\begin{array}{l} H(\omega) = H_c(\omega) \\[2mm] \left|H(\omega)\right| = \gamma(\omega)\left|H_s(\omega)\right| \end{array}\right\} \qquad (50)$$

Noise in both input and output.- If noise $n_1(t)$ is present in the input and noise $n_2(t)$ is present in the output, the estimates obtained are:

$$\left.\begin{array}{l} \left|H_s(\omega)\right|^2 = \dfrac{\Phi_z(\omega) + \Phi_{n_2}(\omega) + 2R\left[\Phi_{zn_2}(\omega)\right]}{\Phi_x(\omega) + \Phi_{n_1}(\omega) + 2R\left[\Phi_{xn_1}(\omega)\right]} \\[5mm] H_c(\omega) = \dfrac{\Phi_{xz}(\omega) + \Phi_{xn_2}(\omega) + \Phi_{n_1z}(\omega) + \Phi_{n_1n_2}(\omega)}{\Phi_x(\omega) + \Phi_{n_1}(\omega) + 2R\left[\Phi_{xn_1}(\omega)\right]} \end{array}\right\} \qquad (51)$$

For noises incoherent to the signals and to each other, these equations reduce to

$$
\left.
\begin{aligned}
\left| H_s(\omega) \right|^2 &= \frac{\Phi_z(\omega) + \Phi_{n_2}(\omega)}{\Phi_x(\omega) + \Phi_{n_1}(\omega)} \\[2em]
H_c(\omega) &= \frac{\Phi_{xz}(\omega)}{\Phi_x(\omega) + \Phi_{n_1}(\omega)}
\end{aligned}
\right\}
\tag{52}
$$

For $\Phi_{n_1}(\omega) \ll \Phi_x(\omega)$ and $\Phi_{n_2}(\omega) \ll \Phi_z(\omega)$, equations (52) become

$$
\left.
\begin{aligned}
\left| H_s(\omega) \right|^2 &\approx \left| H(\omega) \right|^2 \left[1 + \frac{\Phi_{n_2}(\omega)}{\Phi_z(\omega)} \right]\left[1 - \frac{\Phi_{n_1}(\omega)}{\Phi_x(\omega)} \right] \\[2em]
H_c(\omega) &\approx H(\omega) \left[1 - \frac{\Phi_{n_1}(\omega)}{\Phi_x(\omega)} \right]
\end{aligned}
\right\}
\tag{53}
$$

Equations (53) indicate that the noises may be self-balancing in the spectral case whereas only the input noise affects the cross-spectral case.

If significant noises are present in both the input and output, the coherency function is given by

$$
\gamma^2(\omega) = \frac{\left| \Phi_{xz}(\omega) + \Phi_{xn_2}(\omega) + \Phi_{n_1 z}(\omega) + \Phi_{n_1 n_2}(\omega) \right|^2}{\left\{ \Phi_x(\omega) + \Phi_{n_1}(\omega) + 2R\left[\Phi_{xn_1} \right] \right\} \left\{ \Phi_z(\omega) + \Phi_{n_2}(\omega) + 2R\left[\Phi_{zn_2}(\omega) \right] \right\}}
\tag{54}
$$

which, for the incoherent case, reduces to

$$
\gamma^2(\omega) = \frac{1}{\left[1 + \frac{\Phi_{n_1}(\omega)}{\Phi_x(\omega)} \right]\left[1 + \frac{\Phi_{n_2}(\omega)}{\Phi_z(\omega)} \right]}
\tag{55}
$$

or

$$\gamma^2(\omega) \approx 1 - \frac{\Phi_{n_1}(\omega)}{\Phi_x(\omega)} - \frac{\Phi_{n_2}(\omega)}{\Phi_z(\omega)} \tag{56}$$

for $\Phi_{n_1}(\omega) \ll \Phi_x(\omega)$ and $\Phi_{n_2}(\omega) \ll \Phi_z(\omega)$, the reduction in coherency being in proportion to the sum of the ratios of noise power to signal power for both the input and output.

Examination of the results given by equations (53) to (56) indicates that, in the case of noise present in both the input and output, uncontaminated estimates of $H(\omega)$ can no longer be recovered directly from the contaminated estimates as was the case for only one noise. Additional information on the magnitudes of the two ratios of noise power to signal power is required for such corrections. Such supplementary information may sometimes be available to permit corrections for these distortions to be made. For example, certain types of film-record reading errors have been studied and were found to have roughly white power spectra with root-mean-square reading errors of about 0.003 inch of film deflection. Corrections for such effects are actually explored subsequently in regard to the results given in part I.

(It should be noted that the designation of the input and output is, from a mathematical viewpoint, arbitrary. Thus $z(t)$ may be considered the input and $x(t)$ the output for a reversed system. This procedure moves the noise from the input to the output or vice versa. However, the results obtained for the estimates of the frequency-response function for the reversed system are equivalent to those obtained for the direct system when the appropriate corrections for the distortions due to noise are applied.)

The foregoing cases of noise contamination all lead to significant reductions in the coherency function and, aside from their effects in introducing distortions, also lead to increased statistical sampling errors as indicated by figure 15.

Effect of Additional Gust Components

Some airplane responses may be affected by more than one gust component. For example, in addition to the vertical component of the turbulence, the longitudinal (head-on) and side components of turbulence may sometimes give rise to significant effects, particularly at low frequencies, on the root bending strains. The following sketch indicates the nature of the case to be considered:
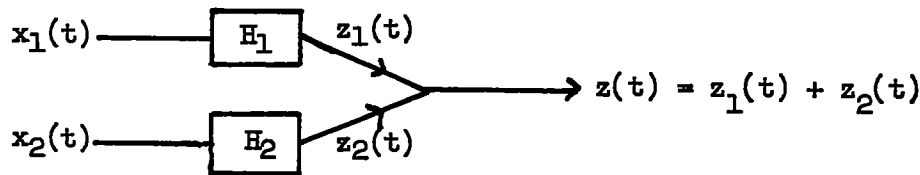
where x_1, for example, is the vertical gust velocity; x_2, the side or head-on gust velocity; and H_1 and H_2 designate the respective frequency-response functions for responses in z. This case will be recognized as a special case of noise in the output as considered in the previous section. For sinusoidal disturbances in $x_1(t)$ and $x_2(t)$ at a given frequency, the amplitude of the response in $z(t)$ is given by

$$Z(\omega) = X_1(\omega) \, H_1(\omega) + X_2(\omega) \, H_2(\omega) \tag{57}$$

where $Z(\omega)$, $X_1(\omega)$, and $X_2(\omega)$ are the Fourier transforms. If equations (27) and (28) are applied to measurements of $x_1(t)$ and $z(t)$ for the purpose of estimating $H_1(\omega)$, the following expressions for the estimates of the frequency-response function are obtained:

$$\left|H_s(\omega)\right|^2 = \left|H_1(\omega)\right|^2 + \frac{\Phi_{x_2}(\omega)}{\Phi_{x_1}(\omega)}\left|H_2(\omega)\right|^2 + \frac{1}{\Phi_{x_1}(\omega)}\left[\Phi_{x_1 x_2}(\omega) \, H_1{}^*(\omega) \, H_2(\omega) + \right.$$

$$\left. \Phi_{x_2 x_1}(\omega) \, H_2{}^*(\omega) \, H_1(\omega)\right] \tag{58}$$

and

$$H_c(\omega) = H_1(\omega) + \frac{\Phi_{x_1 x_2}(\omega)}{\Phi_{x_1}(\omega)} \, H_2(\omega) \tag{59}$$

Thus, both methods lead to contaminated estimates of $H_1(\omega)$. Other methods of estimating the frequency response functions are feasible but require additional study.

For the special case of isotropic turbulence $\Phi_{x_1 x_2}(\omega) = 0$, the results reduce to

$$\left|H_s(\omega)\right|^2 = \left|H_1(\omega)\right|^2 + \frac{\Phi_{x_2}(\omega)}{\Phi_{x_1}(\omega)}\left|H_2(\omega)\right|^2 \tag{60}$$

and

$$H_c(\omega) = H_1(\omega) \tag{61}$$

Thus, the spectrum case yields biased estimates which are too high by an amount that depends upon the product of the ratios of $\dfrac{\Phi_{x_2}(\omega)}{\Phi_{x_1}(\omega)}$ and $\dfrac{|H_2(\omega)|^2}{|H_1(\omega)|^2}$. The cross-spectrum method yields an unbiased estimate and is clearly to be preferred under these circumstances.

The coherency function $\gamma^2(\omega)$ for this case is given by

$$\gamma^2(\omega) = \frac{\left|\Phi_{x_1}(\omega)\,H_1(\omega) + \Phi_{x_1 x_2}(\omega)\,H_2(\omega)\right|^2}{\Phi_{x_1}(\omega)\left[\Phi_{x_1}(\omega)|H_1(\omega)|^2 + \Phi_{x_2}(\omega)|H_2(\omega)|^2 + \Phi_{x_1 x_2}(\omega)\,H_1^*(\omega)\,H_2(\omega) + \Phi_{x_2 x_1}(\omega)\,H_2^*(\omega)\,H_1(\omega)\right]} \tag{62}$$

which in the incoherent case, which applies to isotropic turbulence, reduces to

$$\gamma^2(\omega) = \frac{1}{1 + \dfrac{\Phi_{x_2}(\omega)}{\Phi_{x_1}(\omega)}\dfrac{|H_2(\omega)|^2}{|H_1(\omega)|^2}} \tag{63}$$

Thus, in order to insure high coherency, it is necessary that

$$\Phi_{x_1}(\omega)|H_1(\omega)|^2 \gg \Phi_{x_2}(\omega)|H_2(\omega)|^2 \tag{64}$$

or that the predominant part of the response in $z(t)$ arises from the disturbance $x_1(t)$.

Two-Dimensional Turbulence

If the vertical turbulence varies across the airplane span or is two-dimensional $w(t,y)$ and equations (27) and (28) are applied to measurements of a response $z(t)$ and the gust input measured at a point, for example, on the airplane center line $w(t,0)$, then serious distortion in the estimates of the frequency-response function may be introduced. As indicated in reference 8, the estimates $|H_s(\omega)|^2$ and $H_c(\omega)$ in this case are defined by

$$|H_s(\omega)|^2 = \frac{\int_{-b/2}^{b/2} \int_{-b/2}^{b/2} \Phi_w(\omega,y_2-y_1)\, H(\omega,y_1)\, H^*(\omega,y_2)\, dy_1\, dy_2}{\Phi_w(\omega,0)} \tag{65}$$

and

$$H_c(\omega) = \frac{\int_{-b/2}^{b/2} \Phi_w(\omega,y)\, H(\omega,y)\, dy}{\Phi_w(\omega,0)} \tag{66}$$

where

b airplane span

$\Phi_w(\omega,y)$ cross-spectrum between vertical-gust velocities at stations 0 and y

$\Phi_x(\omega,y_2-y_1)$ cross-spectrum between gust velocity at span positions y_1 and y_2 for isotropic turbulence

$H(\omega,y)$ influence frequency-response function designating the airplane response to unit sinusoidal gusts at station y

Thus, for the case of two-dimensional turbulence, equations (65) and (66) yield average forms of the influence-type function $H(\omega,y)$ where the averaging differs in the two cases and depends upon the span, the gust spectrum, and the variations with y of the influence functions $H(\omega,y)$. It is clear that, if spanwise variations in turbulence exist, the estimates for the frequency-response function $H(\omega)$ for gusts uniform across the span can be seriously distorted.

A rough estimate of the effects of these spanwise variations in turbulence on the estimates of $H(\omega)$ was derived in reference 8 and is

repeated herein in order to indicate the order of magnitude of the dis-
tortions that may be expected from this source. For this purpose, it is
assumed that

$$H(\omega,y) = H(\omega)\Gamma(y) \tag{67}$$

where $H(\omega)$ is the response to unit sinusoidal gusts that are uniform
across the span and $\Gamma(y)$ may be viewed as a span-position weighting
factor $\left(\int_{-b/2}^{b/2} \Gamma(y)\ dy = 1\right)$. This assumption is an oversimplification
but serves the present purpose of assessing the magnitude of the span-
wise effects. Substituting equation (67) into equations (65) and (66)
yields

$$\left.\begin{array}{l} \left|H_s(\omega)\right| = \left|H(\omega)\right| \bar{\Gamma}_1(\omega) \\[2mm] H_c(\omega) = H(\omega)\bar{\Gamma}_2(\omega) \end{array}\right\} \tag{68}$$

where

$$\left.\begin{array}{l} \bar{\Gamma}_1{}^2(\omega) = \dfrac{\displaystyle\int_{-b/2}^{b/2}\int_{-b/2}^{b/2} \Phi_w(\omega,y_2-y_1)\Gamma(y_1)\Gamma(y_2)\ dy_1\ dy_2}{\Phi_w(\omega,0)} \\[6mm] \bar{\Gamma}_2(\omega) = \dfrac{\displaystyle\int_{-b/2}^{b/2} \Phi_w(\omega,y)\Gamma(y)\ dy}{\Phi_w(\omega,0)} \end{array}\right\} \tag{69}$$

The quantities $\bar{\Gamma}_1(\omega)$ and $\bar{\Gamma}_2(\omega)$ given by equation (69) were evaluated
for an assumed spectrum for isotropic atmospheric turbulence and a uni-
form variation of $\Gamma(y)$ on the basis of results given in reference 13.
A value of 0.1 was assumed for the ratio of the airplane span b to the
scale of turbulence L. The results obtained are shown in figure 16 and
are an indication of the distortions in estimating $H(\omega)$ due to the
spanwise variations in turbulence that may be expected for the two methods.
Note that phase estimates obtained by the cross-spectral method are not
affected by the spanwise variations in turbulence.

The results shown in figure 16 for $\bar{\Gamma}_1(\omega)$ and $\bar{\Gamma}_2(\omega)$ were applied to the estimates of the frequency-response function for the center-of-gravity normal acceleration obtained by the spectrum and cross-spectrum methods (see fig. 11(a)). The adjusted results are shown in figure 11(b). The close agreement between the two adjusted results between the frequencies of about 0.25 and 2 cycles per second lends credence to the foregoing argument on span effects and implies that the spanwise variations in the turbulence are the principal source of distortion in the estimates over this frequency region. At the lower and higher frequencies, other factors may also affect the estimates.

The coherency function between the gust velocity $w(t,0)$ and the response can be obtained from equations (29), (30), and (68) and is given by

$$\gamma^2(\omega) = \frac{\bar{\Gamma}_2^2(\omega)}{\bar{\Gamma}_1^2(\omega)} \qquad (70)$$

From the results of figure 16, it can be seen that $\gamma^2(\omega)$ has a value of 1 at zero frequency and decreases to about 0.90 at 1 cps and to about 0.80 at 3 cps.

More detailed information on the function $H(\omega,y)$ can unfortunately not be recovered from measurements of turbulence restricted to $w(t,0)$ but requires more complete measurements of $w(t,y)$. If the turbulence is measured at stations $y_1, y_2, \ldots y_p$ along the span, for a given frequency the following relation applies between the Fourier transforms of the response and the gust inputs at the various span positions.

$$Z(\omega) = W(\omega,y_1)\, H(\omega,y_1) + \ldots + W(\omega,y_p)\, H(\omega,y_p) \qquad (71)$$

This relation leads to the following linear relations for the cross-spectra between the various gust inputs and the response $\Phi_{w_i z}(\omega)$:

$$\Phi_{w_i z}(\omega) = \sum_{k=1}^{p} \Phi_{w_i w_k}(\omega)\, H(\omega,y_k) \qquad (i = 1, 2, \ldots p) \quad (72)$$

where $\Phi_{w_i w_k}(\omega)$ is the cross-spectrum between the gust inputs at stations y_i and y_k. Measurements of $\Phi_{w_i z}(\omega)$ and $\Phi_{w_i w_k}(\omega)$ may in principle be used in these p linear equations to solve for the

p functions $H(\omega, y_k)$ representing the frequency-response function of the system to unit sinusoidal gusts at position y_k. The application of equation (72) would presumably require long sample times inasmuch as the individual coherency functions between the gust velocities $w(t,y)$ and $z(t)$ would be low. Another condition on this approach is the requirement for significant spanwise variations in the turbulence. These variations may be difficult to obtain in flight tests but are perhaps easier to realize in wind-tunnel tests.

RELIABILITY OF PRESENT TEST RESULTS

In this section of the paper, the preceding analysis is applied in assessing the reliability of the test results of part I. For this purpose, various noises believed to be present in the measurements are examined and their effects on the coherency, power spectra, and frequency-response functions are evaluated. The principal aim of this assessment is to establish the magnitude of the possible bias or distortion introduced in the frequency-response functions and to determine their statistical sampling reliability.

The analysis indicates that the coherency functions between the gust input and the strain responses provide an indication of the possible presence of distortions arising from noise and also control the size of the sampling error. For these reasons, the discussion will commence with an examination of the noise sources that may be expected to yield reductions in the coherency function. It will be helpful in reading the following material to keep in mind that noise in either the input or output reduces the coherency. However, only input noises introduce distortions in the frequency-response functions obtained by the cross-spectral method which will be of principal concern. Estimates of the reduction in coherency function due to various noise sources are derived. These estimates for the coherency function are then compared with the values of coherency determined directly from the test measurements as a check on the consistency of this analysis with the test data. The magnitudes of the associated distortions in the measured frequency-response functions and the sampling errors are then considered.

Coherency Function

The principal noise sources giving rise to reductions in coherency and bias in the present frequency-response functions are believed to be the following:

(a) Instrument errors

(b) Record reading errors

(c) Extraneous disturbances

    (1) Longitudinal (head-on) gusts

    (2) Lateral (side) gusts

    (3) Spanwise variations in vertical turbulence

    (4) Pilot control motions.

A crude assessment of the effects of these noise sources was made and indicates that each of these factors might be expected to yield significant reductions in the coherency functions at least over a part of the frequency range of concern. The magnitude of these reductions in coherency between the gust velocity and the various strain responses varied somewhat inasmuch as these reductions, in general, depend upon the ratio of the power spectrum of the strain response (or input) arising from the noise source to the uncontaminated power spectrum of the strain (or input). Representative or average values for the percent reductions in the coherency arising from each noise source are shown in the following table:

Noise source	Estimated percent reductions in the coherency functions by noise source for frequencies of -			
	<0.3 cps	0.3 to 2 cps	2 to 3 cps	>3 cps
Instrument errors . .	--	---------	?	?
Reading errors . . .	0	0 to 10	10 to 25	25
Side gusts	20	---------	---------	--
Head-on gusts	10	10	10	10
Spanwise gust variations	10	5 to 20	20 to 30	30
Pilot control motions	10	---------	---------	--
Total	50	15 to 40	40 to 65	65

where the dashed lines indicate a negligible reduction. Of the six noise sources listed in the table, three (side gusts, head-on gusts, and control motions) are believed to affect only the output measurements whereas the other three affect both the input and output, and the noise in both was

considered. The overall reductions shown in the last row of the table are obtained simply by an addition of the reductions due to individual errors. It is worth noting some of the considerations involved in arriving at the estimates for the individual values given in the table.

The instrument errors were generally considered to be negligible except for frequencies above 3 cps. As indicated by the instrument characteristics given in table II, most of the instruments employed, as well as the recorders, had high natural frequencies above 10 cps and high damping. The frequency-response functions for all instruments were thus essentially flat to 5 cps for most of the important instruments. Phase shifts introduced by the instruments were sufficiently small to be considered negligible, below 2 or 3 cps. The overall accuracy values quoted in table II for the various measurements are based upon static and dynamic bench tests of the recorders. In general, the accuracies quoted were below the levels of the reading error.

One exception to this satisfactory instrument situation is the vane measurements of angle of attack. Measurements of the angle of attack indicated a noticeable oscillation at about 6 cps which appears to be associated with the natural bending frequency of the boom. The level of this oscillation was sufficiently high to mask the angle-of-attack variations at frequencies above 3 cps for low-altitude tests and at even lower frequencies at high altitudes. As a consequence, the high-altitude gust data were not used and the low-altitude gust data are considered suspect at frequencies above 3 cps and possibly also between 2 and 3 cps. No quantitative estimates could be made for this effect, and for this reason the table shows a question mark for the higher frequencies. Fortunately, in most cases, the strain responses above 2 cps were small and therefore this limitation is not too serious for the low-altitude tests.

When the effects of reading errors were considered, estimates of the power spectrum and the root-mean-square value of the reading error were obtained by determining the power spectra of the differences between repeated readings of some of the present records. The results obtained indicate that the power spectrum of the reading error was flat over most of the frequency range with a root-mean-square value of 0.003 inch of film deflection. This result is in agreement with results obtained in other investigations. There was some evidence to suggest that the method of reading which involved periodic adjustment of a reference level introduces additional power to the spectrum of reading error at the lower frequencies. The magnitude of the additional error is difficult to specify and appears to vary widely. Except for this condition at the very low frequencies, the effects of reading error can be estimated reasonably well.

The estimated root-mean-square values of the reading error for the various quantities are summarized in table IV and indicate that in almost all cases the root-mean-square reading error σ_e was less than 10 percent of the true root-mean-square value for the quantity. Inasmuch as a root-mean-square reading error of 10 percent of the true root-mean-square value yields only a one-half percent increase in the measured root-mean-square value, the effects of the reading error on the root-mean-square values are negligible, as can be seen from the results of table IV. The amplification A shown in this table of the true root-mean-square value σ_{true} due to reading error indicates that in almost every case the error is less than about 1 percent.

Although the reading error has a small effect on the root-mean-square values, the ratio of the power spectrum of the reading error to the power spectrum of the uncontaminated strains appears to be sizable at the higher frequencies for most of the measurements. The associated reduction in coherency may, therefore, be expected to be large at the higher frequencies in many cases. For the strain and acceleration measurements, the effects of reading error appear to be negligible over the frequency region from 0 to 2 cps. At higher frequencies, these errors become more important because of the lower power levels for the responses and the flat character of the reading-error spectrum. A reduction of about 5 percent at 3 cps is estimated to arise from this source. At higher frequencies, the reduction may be expected to increase rapidly.

The effects of reading errors on the gust velocity also appear to be significant. The rapid decrease with frequency in the spectra of both the gust velocity and the vane angle-of-attack error and the low sensitivity of the vane (1/10 inch of film deflection per degree angle-of-attack change) result in relatively high values for the ratios of the noise power to signal power at the higher frequencies. For the vane angle-of-attack measurements, this ratio is estimated to increase slowly with frequency to 0.1 at 2 cps but then it increases rapidly to 0.20 at 3 cps and to higher values at frequencies above 3 cps. The values given in the preceding table represent estimates of the combined effects of the reading errors in the input and output measurements.

The airplane wing strain responses to side gusts and head-on gusts can normally be expected to be small except at very low frequencies. (For isotropic turbulence, which approximates atmospheric conditions, the strains from these sources can be expected to be incoherent with the strains arising from vertical gusts.) For the side gust case, significant strain responses may be excited in the neighborhood of the Dutch roll mode of the airplane which, in this case, was centered at about 0.16 cps. These effects can be expected to be more pronounced at the outboard stations. The airplane strain responses to head-on gusts are likewise generally small except possibly at frequencies in the

neighborhood of the airplane phugoid oscillation. Rough estimates of the magnitude of these responses were used with equation (63) to arrive at the estimates shown in the foregoing table.

The effects of spanwise variations in the turbulence on the strains are difficult to evaluate accurately. The crude analysis developed for the spanwise effects is, however, believed to yield estimates of at least the order of magnitude of these effects on the coherency between the vertical gust velocity and the strain and acceleration responses. The value in the table is based on the results in figure 16 and equation (70). These estimates should apply best to the root strains and center-of-gravity acceleration because of the assumptions in their derivation. In addition, an arbitrary value of 10 percent is given in the table for the very low frequencies to account for the contributions to the strains arising from asymmetries in the vertical turbulence.

The effects of control motions were evaluated by an examination of the records obtained with the control-position recorders. In the overall, the pilots made infrequent use of the control surfaces during the gust tests. The control motions were largely restricted to a few aileron control movements, presumably to correct for deviations in the airplane roll attitude. These control motions were, in general, slowly applied and are not believed to affect the coherency functions at frequencies above 3/10 cps.

In order to determine how well the foregoing estimates approximate the actual conditions, figure 17 shows a comparison of representative coherency functions obtained directly from the test measurements with those given by the results of the foregoing table. Figure 17 shows the measured coherency function between the gust input and the outputs of normal acceleration and strains at two stations. For this comparison, a smooth curve was used to approximate the variations of the coherency function with frequency given by the table. In general, the estimates derived appear to approximate the general character of the measured results with a low coherency below 0.30 cps, a relatively high coherency level of 70 to 90 percent between 0.3 cps and 2 cps, and a rapid reduction at the higher frequencies. This consistency implies that the noise structure in the measurements has been approximated reasonably well by the analysis. The distortions introduced in the frequency-response functions by this noise structure are considered next.

Distortions in Measured Frequency-Response Functions

The analysis of the contributions of the various noise sources to the reduction in coherency provides a basis for estimating the bias or distortion in the frequency response arising from these noise sources.

The analysis has indicated that incoherent noise sources in the output introduce no significant distortions in the cross-spectral estimates of the frequency-response function. Thus, it may be expected that effects of side gusts, head-on gusts, and control motions do not significantly affect the frequency-response functions obtained by the cross-spectrum method. This conclusion is particularly applicable to frequencies above 0.30 cps, where present concern is centered, and is perhaps subject to some question at lower frequencies.

The remaining three sources of noise, instrument errors, reading errors, and spanwise gust variations, do however affect the input measurements and, on the basis of the preceding analysis, may be expected to introduce distortions in the estimated frequency-response functions. The principal source of instrument error was associated with the effects of vibrations of the boom on the angle-of-attack measurements. No quantitative measure of the distortions due to this source could be given although it does not appear likely that these vibrations yielded any appreciable error at frequencies below 2 cycles per second.

The reading errors in the gust determination and spanwise variations of turbulence appear to give rise to significant distortions in the estimated frequency-response functions. Based on the analysis of the reductions in the coherency function given in the table, it is estimated that the amplitudes of the frequency-response functions obtained by the cross-spectral method are too low by the percentages given in the following table for the two sources:

Source	Percentage error in amplitude for frequencies of -		
	< 0.3 cps	0.3 to 2.0 cps	2.0 to 3.0 cps
Reading errors	0	0 to 10	10 to 20
Spanwise gust variations . .	0	5 to 20	20 to 30
Total	0	5 to 30	30 to 50

These values are crude estimates but are believed to approximate the actual situation, at least for frequencies between 0.3 and 2 cps. At frequencies between 2 and 3 cps, the strain responses are, in general, very low and thus the large underestimation is not too important. These estimates of the distortion should be applied to the present results (figs. 12 and 13) in order to make direct quantitative comparisons with results obtained in other studies. It is felt that these distortions apply about equally well to the acceleration responses which are used

as reference conditions; thus, these distortions do not affect internal comparisons aimed at establishing the magnitude of the flexibility effects.

The distortion in estimates of the frequency-response function obtained by the spectral method may also be derived on the basis of the preceding analysis. These distortions, in general, would appear to be larger for the spectrum case, particularly at low frequencies, inasmuch as the distortions arising from side gusts, head-on gusts, and control motions would have to be considered in greater detail. In addition, reading errors in the output measurements will also give rise to distortion in the spectrum case whereas in the cross-spectrum case no distortion due to this source occurs. The larger distortions and the difficulty of estimating their magnitudes accurately in the spectral method contribute to making this technique a less satisfactory one than the cross-spectral technique.

The results of figure 11(b), in which the estimates of the frequency-response function obtained by the two methods are adjusted for effects of the spanwise variations in turbulence, show good agreement between frequencies of 0.30 cps to 2 cps. This good agreement implies that the spanwise variations in turbulence are the principal sources of noise error in this frequency region. The discrepancies at both lower and higher frequencies in figure 11(b) are attributed to the effects of the lateral motions and pilot control motions for the low frequencies and the effects of reading errors and instrument errors, particularly in the input, for the very high frequencies.

Statistical Sampling Errors

In order to estimate the statistical reliability of the measured frequency-response functions, the measured coherency functions and the charts in figure 15 were used to derive 90-percent confidence intervals for the frequency-response functions. Figure 18 illustrates typical results obtained and shows the confidence bands for the center-of-gravity acceleration response and the bending-strain response at the front spar at station 54. Examination of figure 18 indicates that, except for the very low and very high frequencies, the amplitudes are reliable to within about ±20 percent of the measured value. At the extreme frequencies (below 0.30 cps and above about 1.80 cps) the amplitudes are far less reliable because of the lower coherency at these frequencies and in some cases are, in fact, so large as to suggest that reliable estimates cannot be obtained in these frequency regions. The phase angles also appear to be very reliable with the confidence bands less than ±10° about the measured values for frequencies between about 0.30 and 2 cps. At the higher and lower frequencies, the confidence bands for the phase angle are also considerably increased because of the lower coherency.

A further verification of the statistical reliability of the present results is indicated by the consistency of the results obtained from the independent estimates made from the two 2-minute samples as illustrated by the results for the center-of-gravity acceleration shown in figure 14.

COMMENTS ON RANDOM-PROCESS TECHNIQUES OF

FREQUENCY-RESPONSE DETERMINATION

A few comments appear to be warranted on the random-process techniques as employed in this study for the determination of airplane frequency-response functions. The results obtained in the present study indicate that reasonably reliable frequency-response functions for airplane responses to rough air may be obtained from full-scale flight tests in continuous turbulence. Two methods were employed for this purpose - the spectral method and the cross-spectral method. The cross-spectral method definitely appears to be preferable, inasmuch as the results obtained with this method are affected less by extraneous disturbances, particularly disturbances affecting the output measurements. These are of particular significance for atmospheric turbulence problems inasmuch as the lateral and longitudinal components of turbulence are always present. In addition, only the cross-spectral method provides phase information.

The analysis indicates that great care is required in the application of random-process techniques in frequency-response determinations and in the interpretation of the results. Extraneous noises may seriously affect the reliability of the results by introducing distortions and by limiting the statistical reliability of the results. In the present investigation, the significant noise sources were reading errors, extraneous gust components, spanwise variations in turbulence, and pilot control motions. For the lower frequencies, which were of particular concern in the present investigation, these noises did not give rise to serious distortions. In addition, it appears possible to estimate the magnitude of the distortions and to correct for them by using the methods developed herein. For the higher frequencies, the effects of these noises were more serious and, in fact, did not permit reliable results to be obtained. Fortunately, the higher frequencies were of only minor concern in the present study.

Improvements in the reliability of the results can be obtained by a number of precautions. These include improvements in instrumentation, particularly in regard to increased sensitivity and adequate frequency response. Efforts to obtain more intense levels of gust input disturbance will also be beneficial. The statistical sampling errors do not

appear to be too serious a difficulty. In the present investigation,
samples of 2-minute duration lead to statistical or sampling uncertainty
of about 10 to 20 percent for the lower frequencies. The magnitude of
these uncertainties can, of course, be reduced by either longer sampling
durations, achievement of higher coherencies, or by averaging estimates
over a wider frequency band.

The results obtained in the present investigation suggest that the
use of random disturbance inputs may also prove to be practical in exper-
imental frequency-response determinations for responses to other types
of disturbances than gust disturbances; for example, control surface
motions and acoustic disturbances. The use of random inputs for these
purposes can provide substantial reduction in testing time when compared
with conventional techniques involving sinusoidal inputs. As compared
with discrete pulse techniques which are frequently used for this purpose,
the random-input techniques appear to provide equivalent levels of
accuracy. In addition, they may offer a number of practical advantages.
These include the ability to control the effects of extraneous disturb-
ances and a more realistic representation of the character of actual
disturbance functions met in practice.

CONCLUDING REMARKS

The foregoing analysis of the strain responses of a large swept-
wing airplane in rough air has indicated that the wing-bending and shear-
strain responses at the various stations are amplified by rather large
amounts because of the dynamic responses of the structure. The amount
of amplification in the bending strains was about 10 to 20 percent at
the root stations but increased to values in excess of 100 percent in
some cases at the midspan stations. The shear strains showed a similar
pattern across the airplane span but also indicate larger variations
between the front and rear spar stations. The large variations in strain
responses across the airplane span indicate that the strain distributions
in gusts are very different under rough-air loading conditions than under
the usual maneuver loadings and warrant detailed and separate considera-
tion in design. In general, the predominant source of strain amplifica-
tion was associated with the excitation of the fundamental wing-bending
mode. However, at the outboard stations and particularly in the case
of the shear strains, significant contributions to the strains arise
from the higher symmetrical and antisymmetrical vibration modes. Thus,
the effects of these higher modes on the strains may also have to be con-
sidered in stress calculations, depending upon the degree of accuracy
required.

A detailed analysis of the reliability of frequency-response func-
tion estimates obtained by random-process techniques, particularly as

affected by extraneous noise, was given. The effects of such noises in giving rise to systematic errors or distortions and random sampling errors were explored and results of general applicability obtained. These results were also applied to the present test data in order to establish their reliability and to derive adjustments for the distortions. The important result obtained is the indication that with appropriate precautions flight tests in rough air of a few minutes duration may be used to obtain reliable estimates of airplane frequency-response functions.

Langley Aeronautical Laboratory,
    National Advisory Committee for Aeronautics,
        Langley Field, Va., March 18, 1958.

REFERENCES

1. Mickleboro, Harry C., and Shufflebarger, C. C.: Flight Investigation of the Effect of Transient Wing Response on Wing Strains of a Twin-Engine Transport Airplane in Rough Air. NACA TN 2424, 1951.

2. Murrow, Harold N., and Payne, Chester B.: Flight Investigation of the Effect of Transient Wing Response on Wing Strains of a Four-Engine Bomber Airplane in Rough Air. NACA TN 2951, 1953.

3. Mickleboro, Harry C., Fahrer, Richard B., and Shufflebarger, C. C.: Flight Investigation of Transient Wing Response on a Four-Engine Bomber Airplane in Rough Air With Respect to Center-of-Gravity Accelerations. NACA TN 2780, 1952.

4. Houbolt, John C., and Kordes, Eldon E.: Structural Response to Discrete and Continuous Gusts of an Airplane Having Wing-Bending Flexibility and a Correlation of Calculated and Flight Results. NACA Rep. 1181, 1954. (Supersedes NACA TN 3006; also contains essential material from TN 2763 and TN 2897.)

5. Shufflebarger, C. C., Payne, Chester B., and Cahen, George L.: A Correlation of Results of a Flight Investigation With Results of an Analytical Study of Effects of Wing Flexibility on Wing Strains Due to Gusts. NACA TN 4071, 1957.

6. Rhyne, Richard H., and Murrow, Harold N.: Effects of Airplane Flexibility on Wing Strains in Rough Air at 5,000 Feet As Determined by Flight Tests of a Large Swept-Wing Airplane. NACA TN 4107, 1957.

7. Rhyne, Richard H.: Effects of Airplane Flexibility on Wing Strains in Rough Air at 35,000 Feet As Determined by a Flight Investigation of a Large Swept-Wing Airplane. NACA TN 4198, 1958.

8. Coleman, Thomas L., Press, Harry, and Shufflebarger, C. C.: Effects of Airplane Flexibility on Wing Bending Strains in Rough Air. NACA TN 4055, 1957.

9. Press, Harry, and Tukey, J. W.: Power Spectral Methods of Analysis and Their Application to Problems in Airplane Dynamics. Vol. IV of AGARD Flight Test Manual, Pt. IVC, Enoch J. Durbin, ed., North Atlantic Treaty Organization, pp. IVC:1 - IVC:41.

10. Chilton, Robert G.: Some Measurements of Atmospheric Turbulence Obtained From Flow-Direction Vanes Mounted on an Airplane. NACA TN 3313, 1954.

11. Salzer, John M.: Frequency Analysis of Digital Computers Operating in Real Time. Proc. I.R.E., vol. 42, no. 2, Feb. 1954, pp. 457-466.

12. Goodman, N. R.: On the Joint Estimation of the Spectra, Cospectrum and Quadrature Spectrum of a Two-Dimensional Stationary Gaussian Process. Scientific Paper No. 10 (BuShips Contract Nobs-72018 (1734-F) and David Taylor Model Basin Contract Nonr-285 (17)), Eng. Statistics Lab., New York Univ., Mar. 1957.

13. Diederich, Franklin W.: The Response of an Airplane to Random Atmospheric Disturbances. NACA TN 3910, 1957.

TABLE I

PERTINENT PHYSICAL CHARACTERISTICS AND

DIMENSIONS OF TEST AIRPLANE

Total wing area, sq ft 1,428
Wing span, ft 116
Wing aspect ratio 9.43
Wing thickness ratio, percent 12
Wing taper ratio 0.42
Wing mean aerodynamic chord, in. 155.9
Wing sweepback (25-percent-chord line), deg 35
Total horizontal-tail area, sq ft 268
Horizontal-tail span, ft 33
Horizontal-tail mean aerodynamic chord, in. 102.9
Horizontal-tail sweepback (25-percent-chord line), deg 35
Airplane weight:
  For tests at 5,000 feet, lb 113,000
  For tests at 35,000 feet, lb 112,000

TABLE II

SUMMARY OF INSTRUMENT CHARACTERISTICS AND ACCURACIES

Quantity measured	Measurement station	Instrument range	Instrument sensitivity	Film speed, in./sec	Natural frequency, f_n, cps, of –		Approximate damping ratio of –		Estimated instrument accuracy –
					Sensing element	Recording element	Sensing element	Recording element	
Normal acceleration, g units	34.2 percent $\bar{c}$	±1	1.01 g/in.	0.25	8.5	(a)	0.7	(a)	0.005
Pitching velocity, radians/sec	25.0 percent $\bar{c}$	±0.25	0.254 $\frac{radians/sec}{in.}$	0.25	6.7	(a)	0.67	(a)	0.005
Vane-indicated angle of attack, radians	79 inches ahead of original nose	±0.5	0.185 $\frac{radians}{in.}$	0.25	10 at 200 mph; 20 at 400 mph	10	$\frac{0.1}{\sqrt{\rho/\rho_0}}$	0.7	0.002
Dynamic pressure, lb/sq ft	140 inches ahead of original nose	0 to 800	Approximately 100 lb/sq ft/in.	0.25	>50	(b)	(c)	(b)	1.0
Static pressure, lb/sq ft	132 inches ahead of original nose	0 to 2,200	Approximately 200 lb/sq ft/in.	0.25	>50	(b)	(c)	(b)	2.0
Time, sec	---------	---------	---------	----	---------	----	---------	----	0.005
Bending and shear strains	Eight locations (see fig. 2)	---------	---------	1.0	(d)	100	(d)	0.67	±3 percent

[a] Optical recording element, $f_n \gg 10$ cps.

[b] Mechanical-optical recording element, $f_n \gg 10$ cps.

[c] Damping adequate for present application of airspeed and altitude data.

[d] Strain gages, $f_n \gg 10$ cps.

TABLE III

STRAIN INDICATION PER g AS DETERMINED IN

SLOW PULL-UPS IN SMOOTH AIR

Wing station	Spar	ϵ_0, strain indication per g for -			
		Bending strain at -		Shear strain at -	
		5,000 ft	35,000 ft	5,000 ft	35,000 ft
54	Front	0.47	0.54	0.15	----
54	Rear	.81	.97	.50	0.53
252	Front	.45	.60	----	----
252	Rear	.43	.55	.19	.29
414	Front	.42	.58	.32	.42
414	Rear	.51	.60	.16	.20
572	Front	.18	.26	.43	.53
572	Rear	.25	.36	.16	.21

TABLE IV

AMPLIFICATION OF ROOT-MEAN-SQUARE VALUES DUE TO RECORD READING ERRORS

Measurement	Station	Spar	$100 \dfrac{\sigma_e}{\sigma_{true}}$ at - (a)		Percent amplification, 100A at - (a)	
			5,000 ft	35,000 ft	5,000 ft	35,000 ft
Bending strain	54	Front	4.3	8.6	0.09	0.37
	54	Rear	2.5	4.6	.03	.11
	252	Front	3.8	4.6	.07	.11
	252	Rear	3.9	4.9	.08	.12
	414	Front	2.5	3.5	.03	.06
	414	Rear	2.5	3.4	.03	.06
	572	Front	11.7	11.8	.68	.70
	572	Rear	9.5	7.4	.45	.27
Shear strain	54	Front	6.6	----	0.22	----
	54	Rear	3.3	11.3	.05	0.64
	252	Front	----	----	----	----
	252	Rear	11.9	7.1	.71	.25
	414	Front	3.5	9.4	.06	.44
	414	Rear	5.6	8.1	.15	.33
	572	Front	7.1	3.2	.25	.05
	572	Rear	14.5	8.8	1.05	.39
Acceleration	Center of gravity		2.6	5.0	0.03	0.11

(a) $\sigma_{meas} \approx \sigma_{true}\left[1 + \dfrac{1}{2}\left(\dfrac{\sigma_e}{\sigma_{true}}\right)^2\right] = \sigma_{true}(1 + A)$ where $A = \dfrac{1}{2}\left(\dfrac{\sigma_e}{\sigma_{true}}\right)^2$.
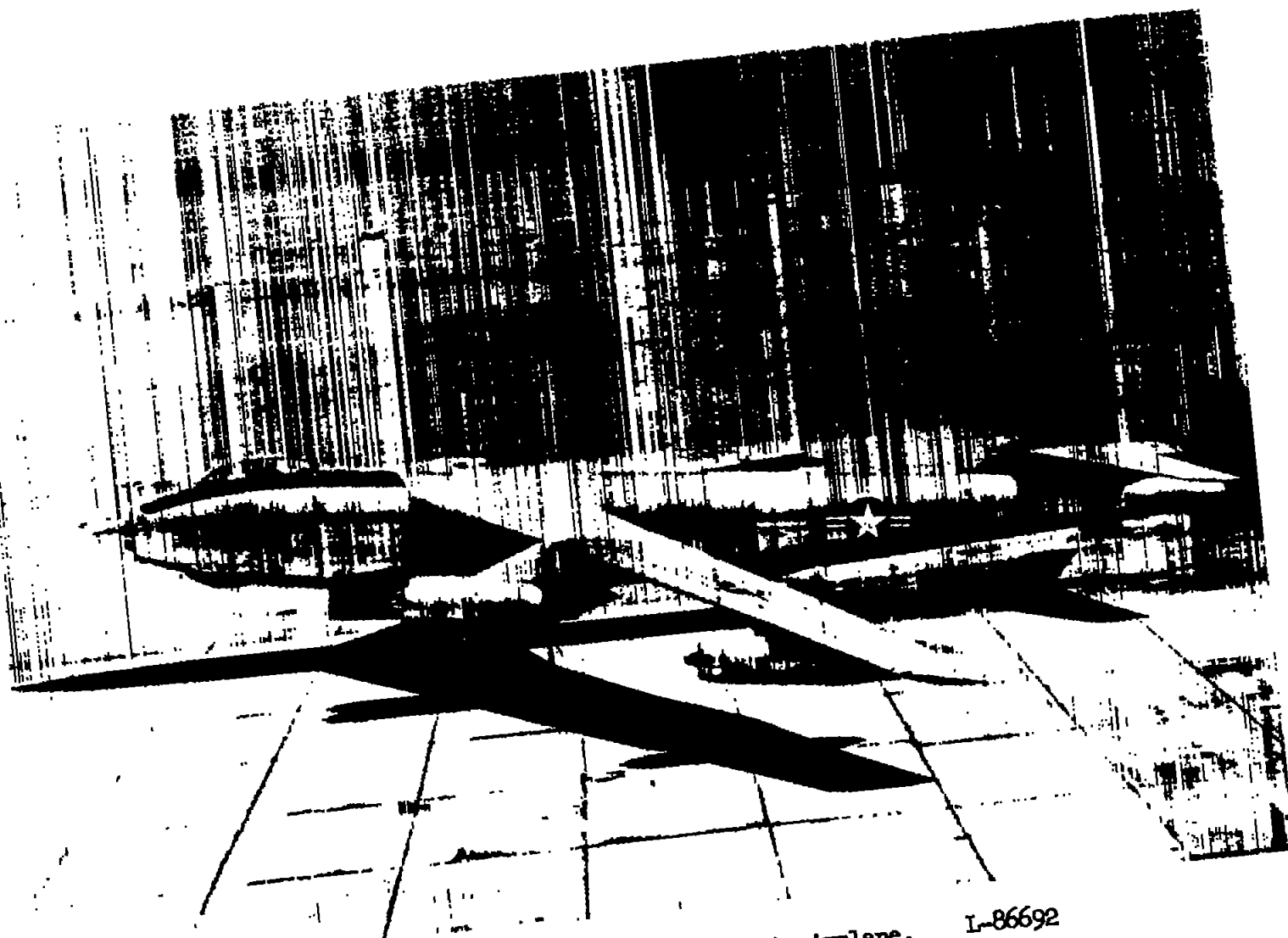
Figure 1.- Photograph of test airplane.   L-86692
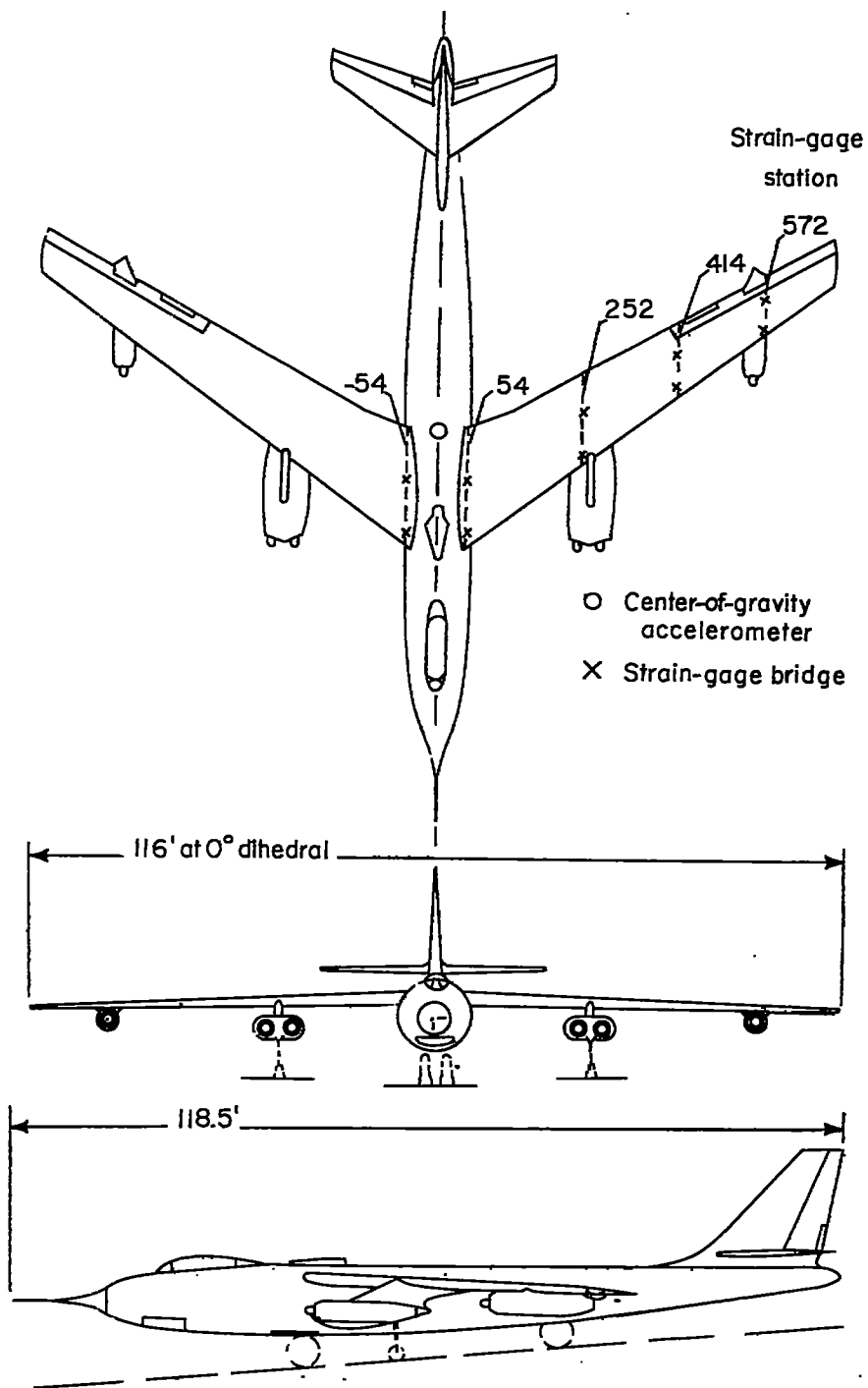
Figure 2.- Three-view drawing of test airplane.
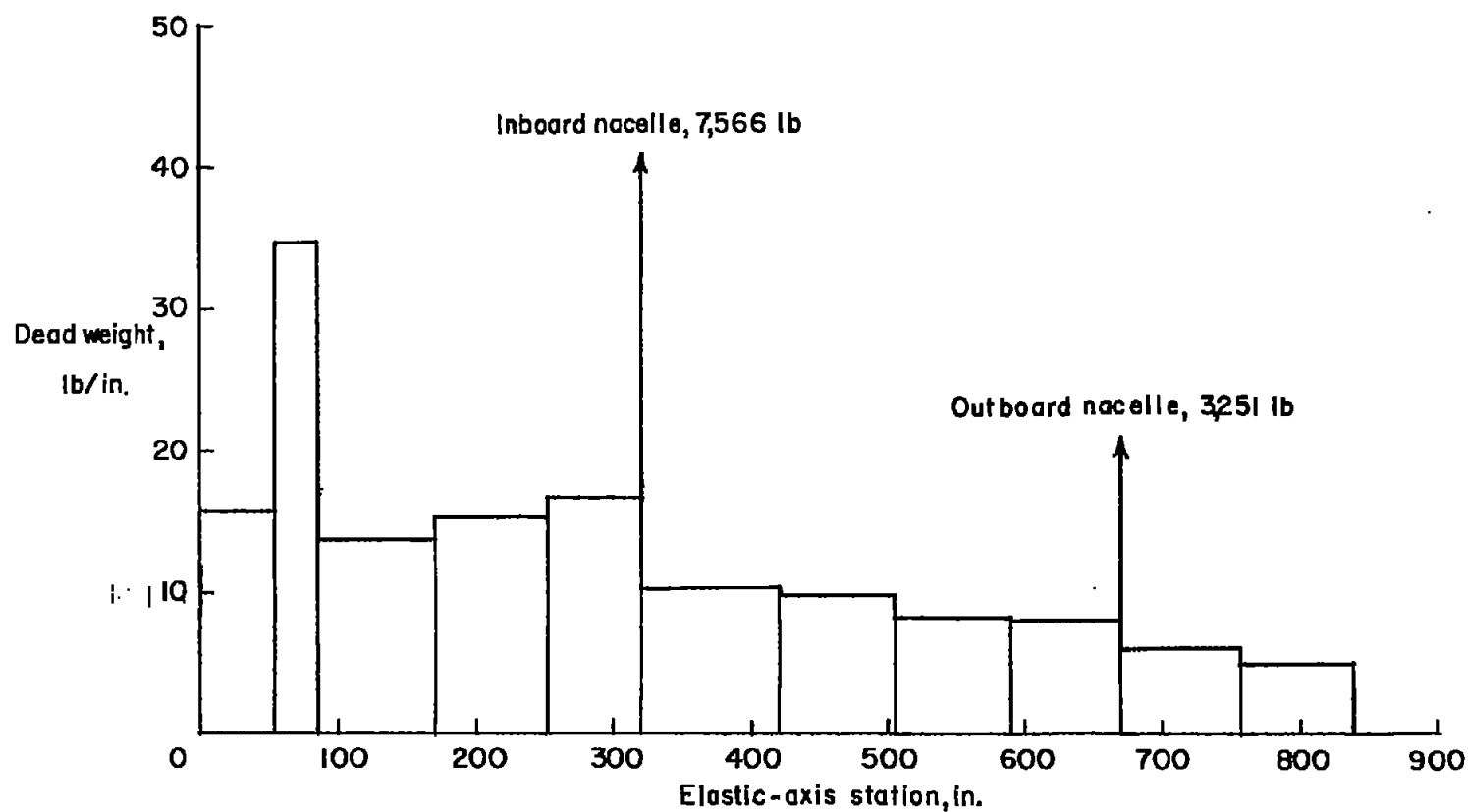
(a) Wing.

Figure 3.- Airplane wing and fuselage weight distributions.
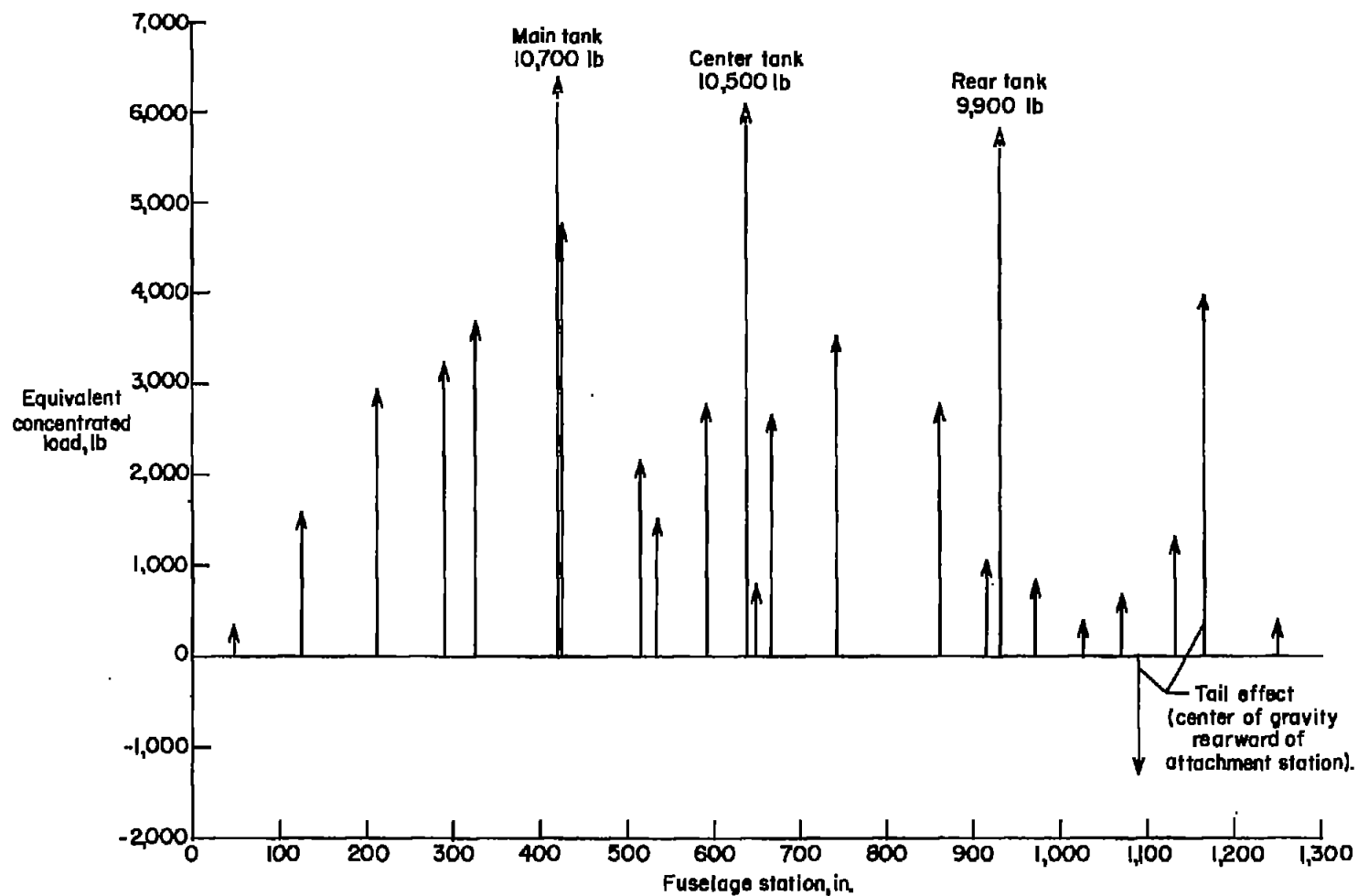
(b) Fuselage.

Figure 3.- Concluded.
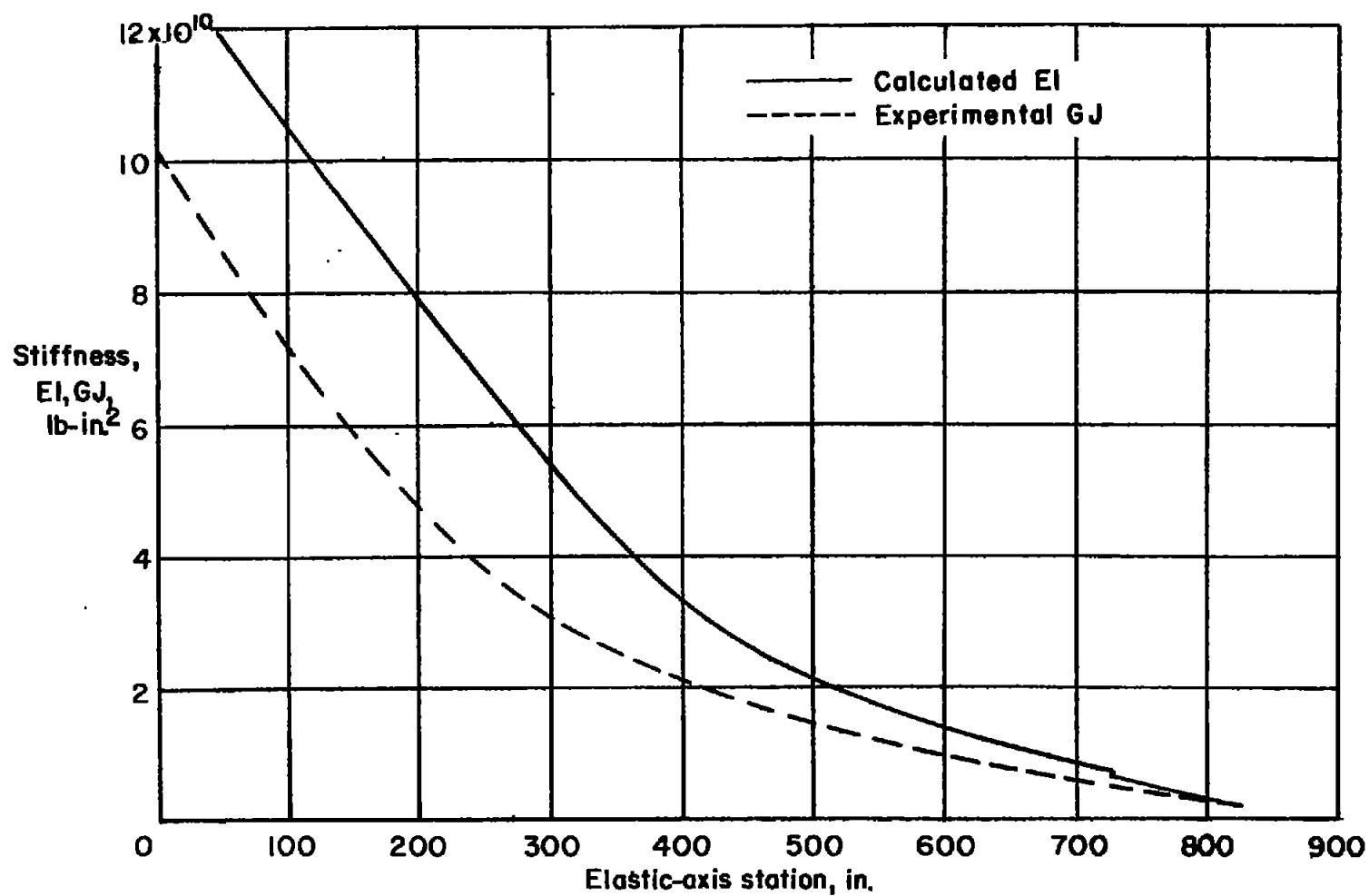
Figure 4.- Bending and torsional stiffness distributions of wing.
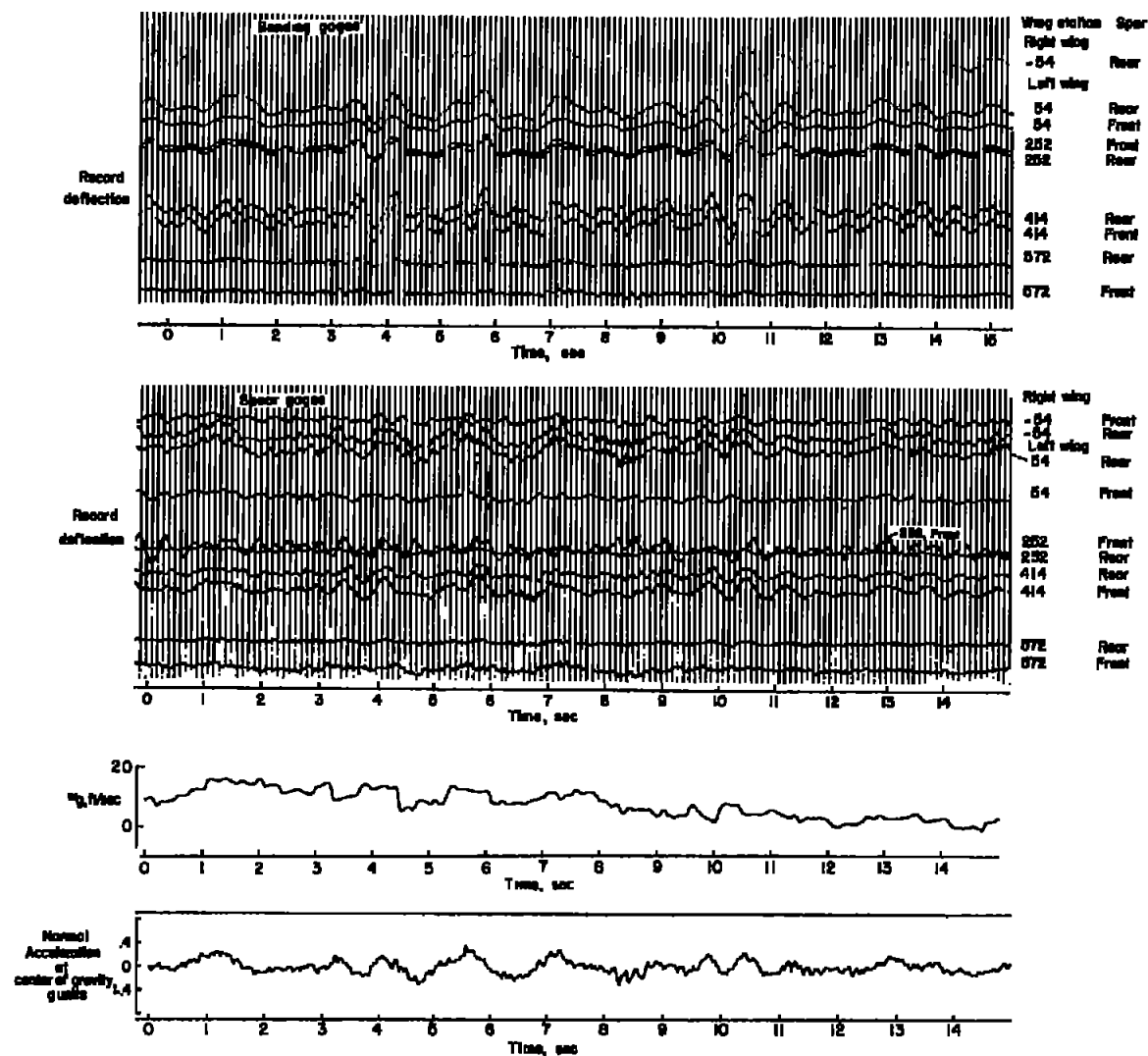
Figure 5.- Portion of time histories of strains, center-of-gravity acceleration, and vertical gust velocity.
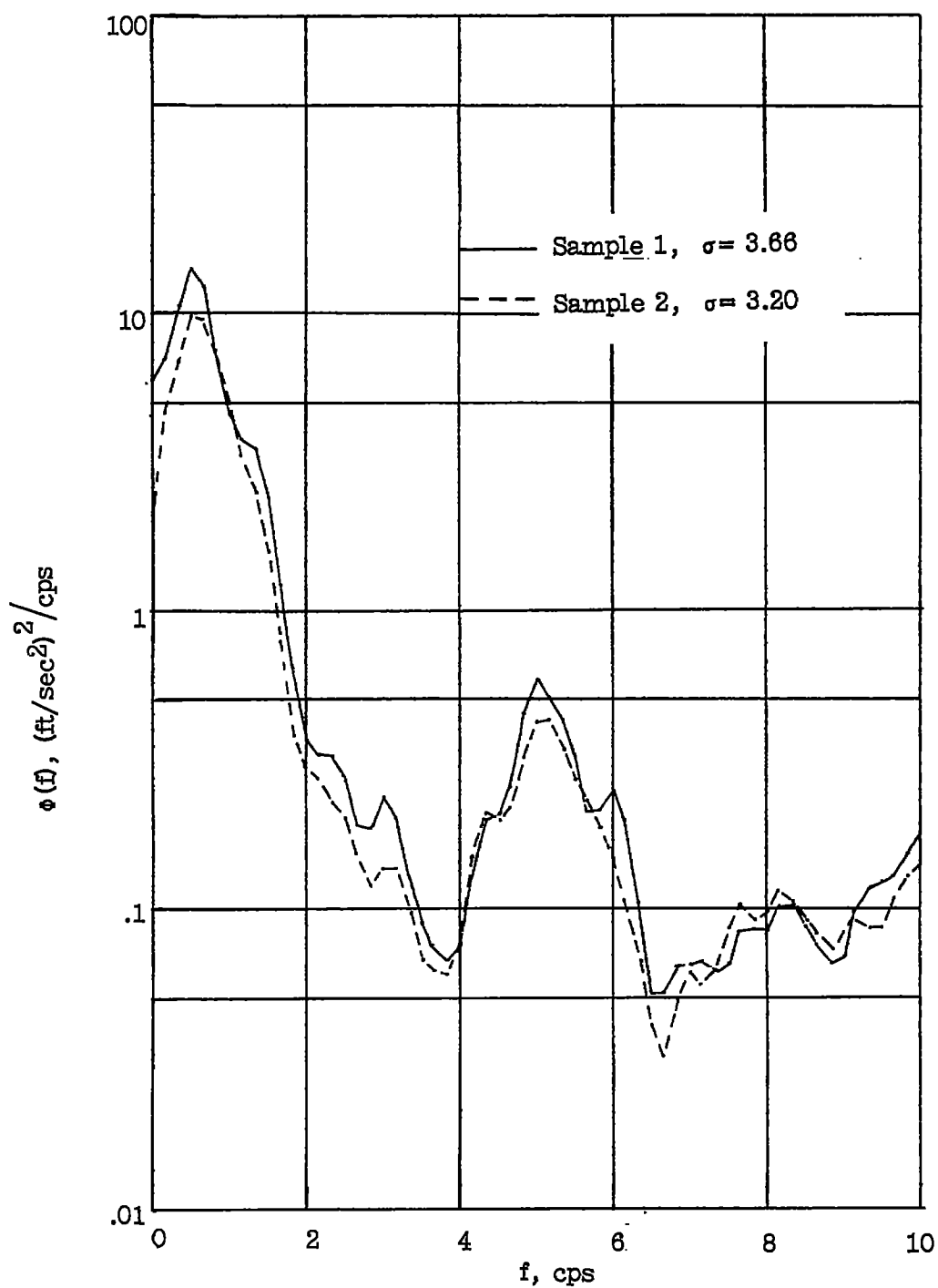
Figure 6.- Comparison of power spectra of measured normal acceleration at center of gravity for two samples.
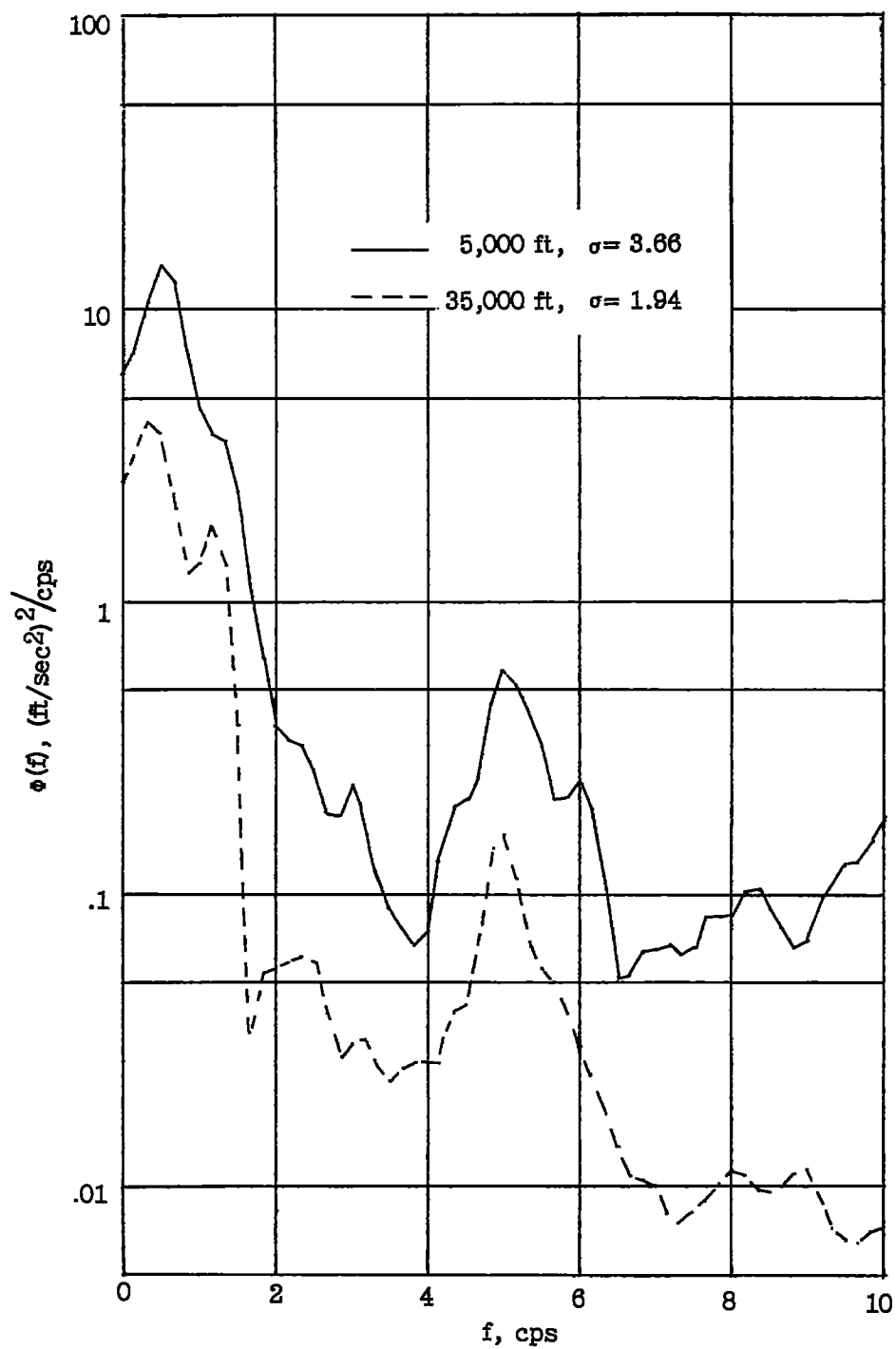
Figure 7.- Comparison of power spectra of measured normal acceleration
at center of gravity for two altitudes.
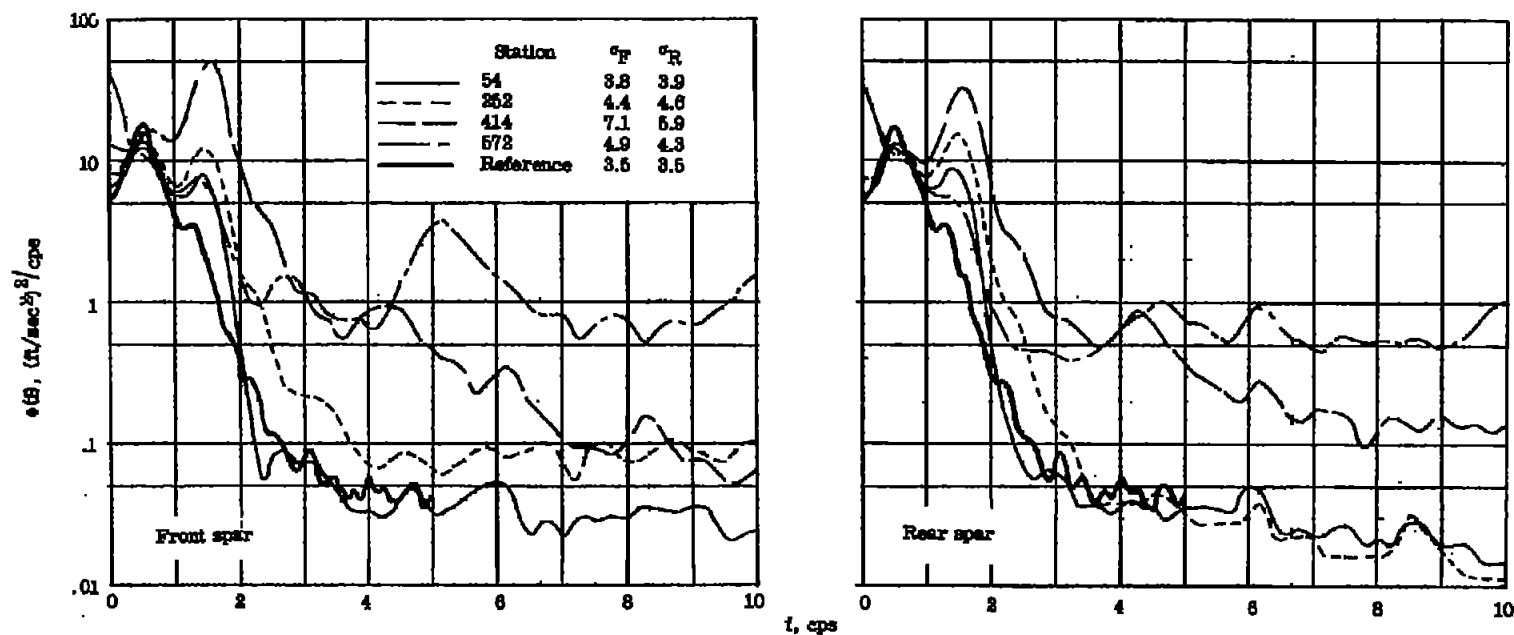
(a) 5,000 feet.

Figure 8.- Power spectra of wing bending strain.
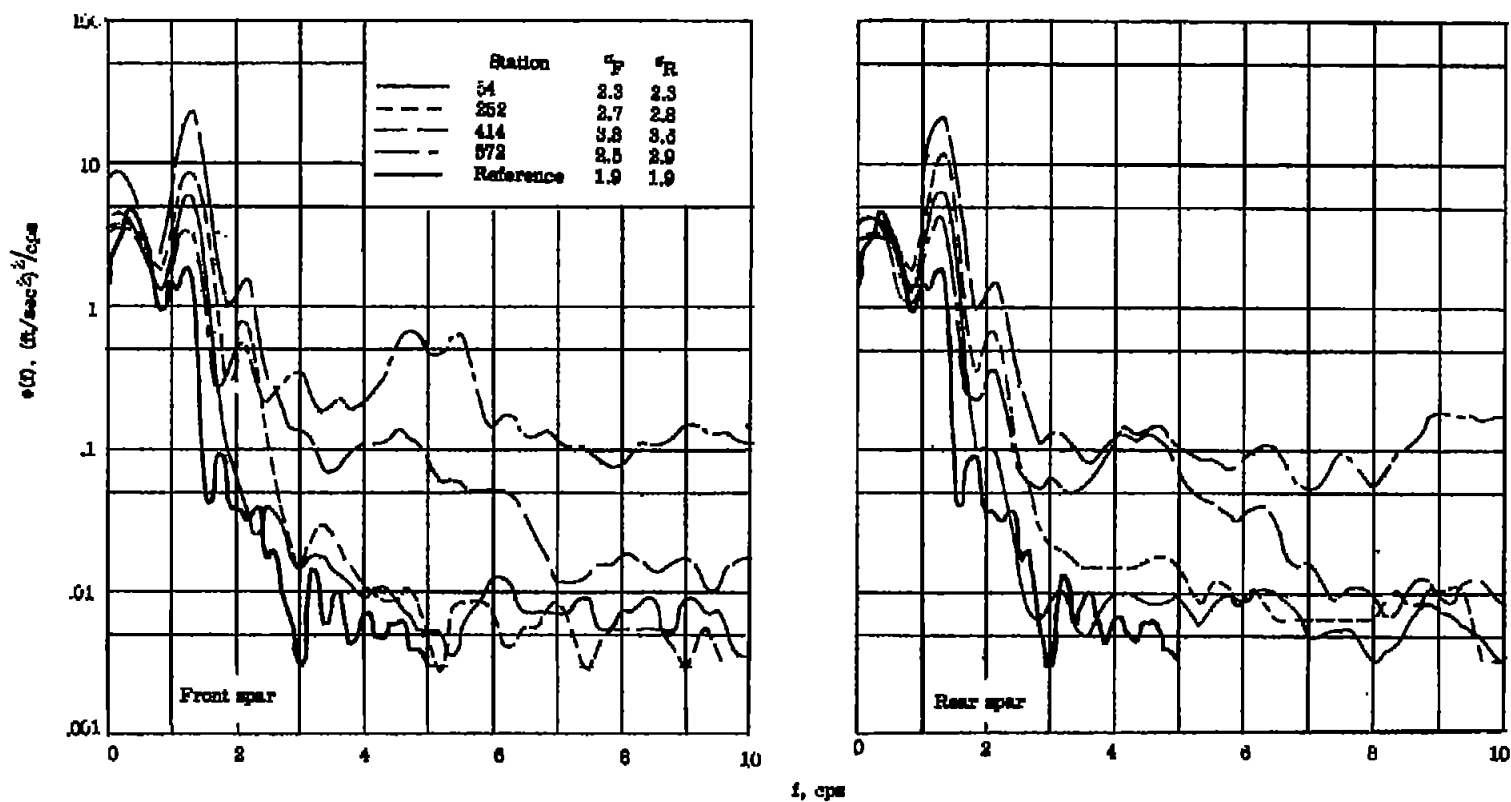
(b) 35,000 feet.

Figure 8.- Concluded.
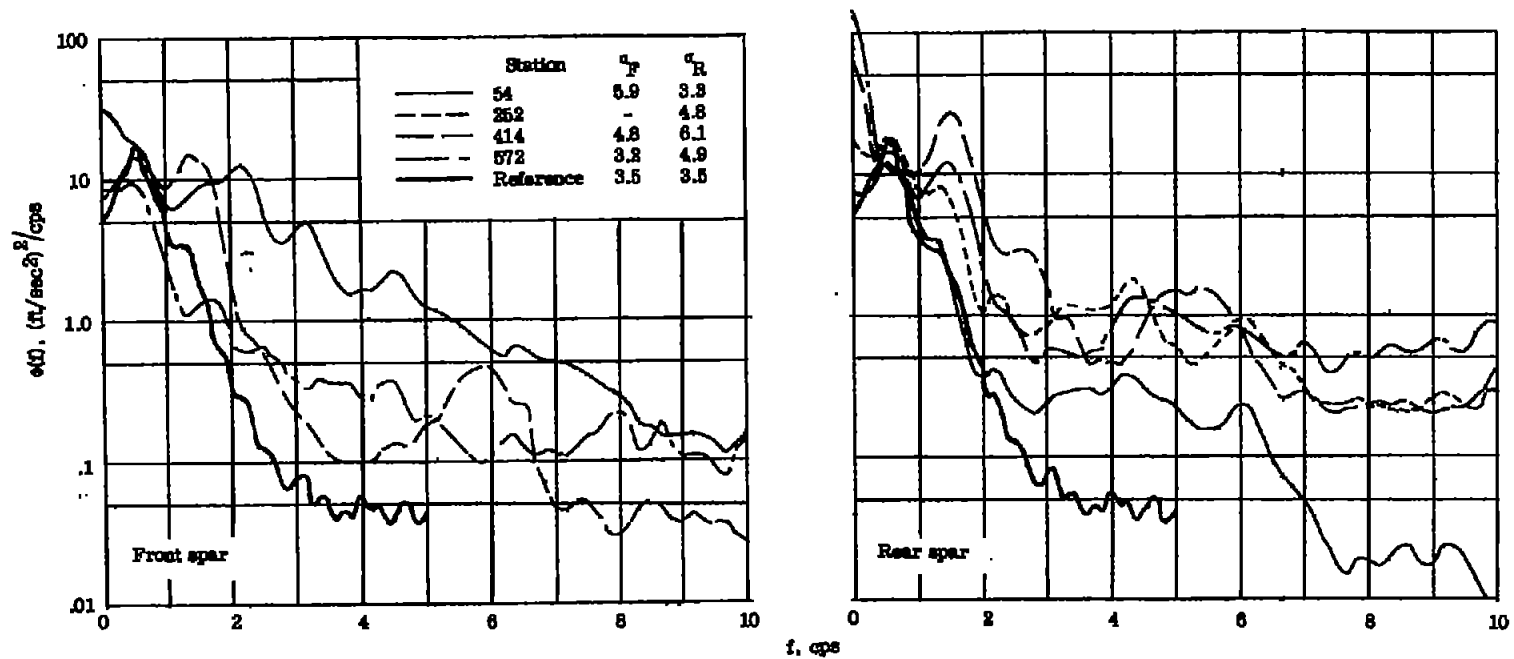
(a) 5,000 feet.

Figure 9.- Power spectra of wing shear strain.
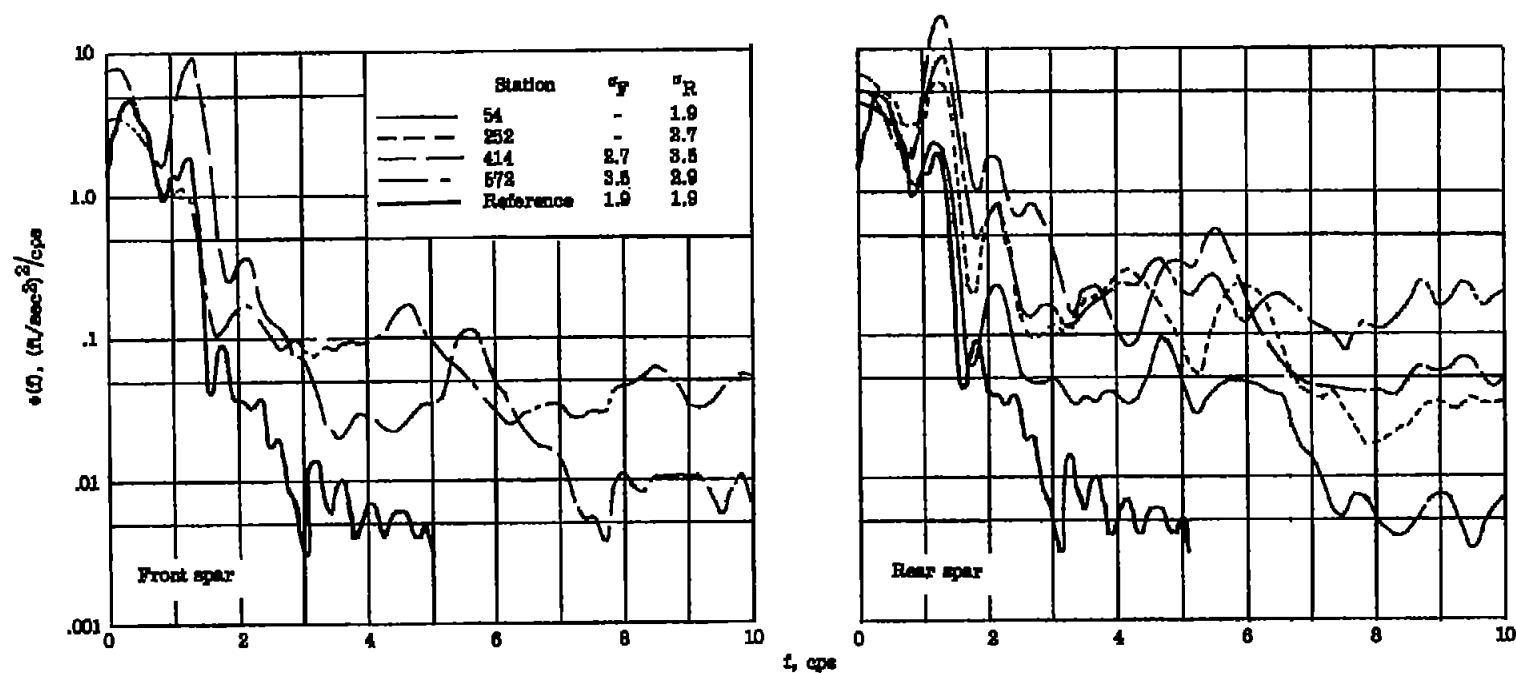
(b) 35,000 feet.

Figure 9.- Concluded.
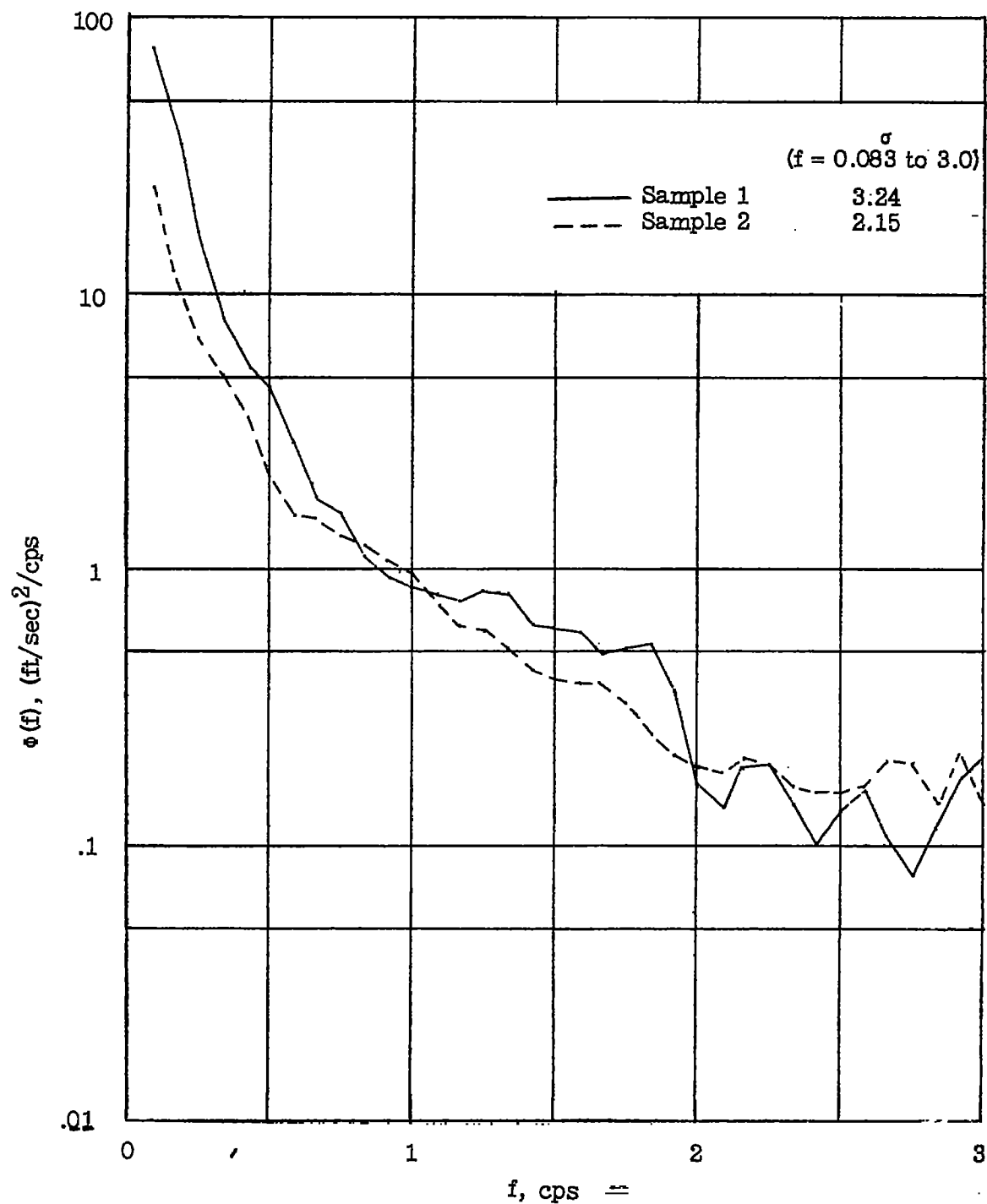
Figure 10.- Comparison of power spectra of vertical gust velocity for
two record samples for low-altitude test.
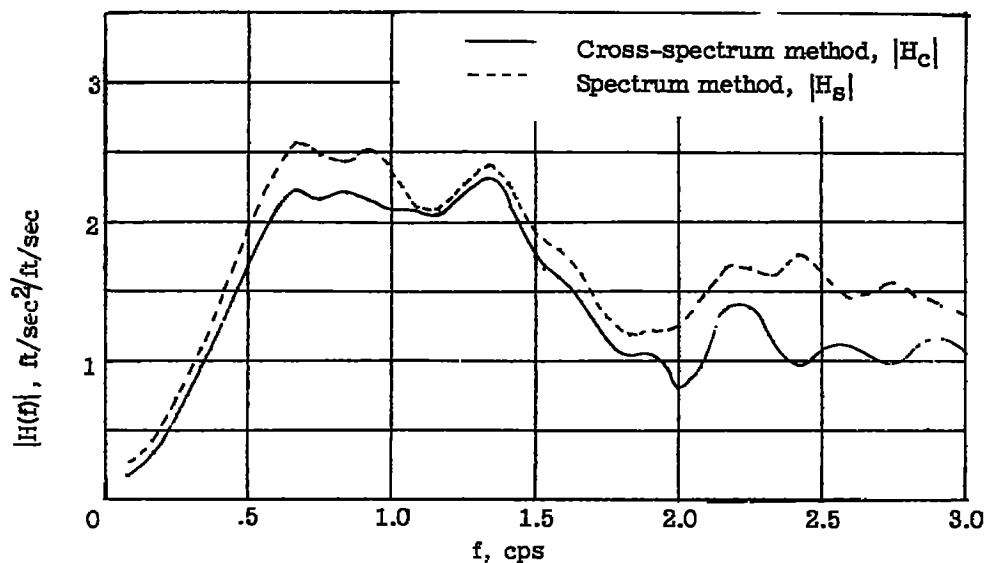
(a) Frequency-response function estimates.
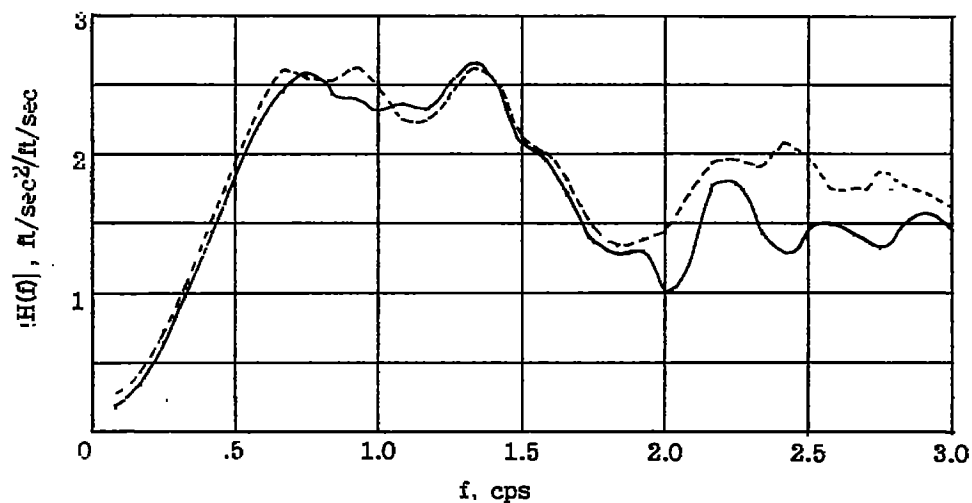
(b) Frequency-response function estimates adjusted for effects
of spanwise variation in turbulence.

Figure 11.- Comparison of frequency-response function estimates
for normal acceleration obtained by two methods.
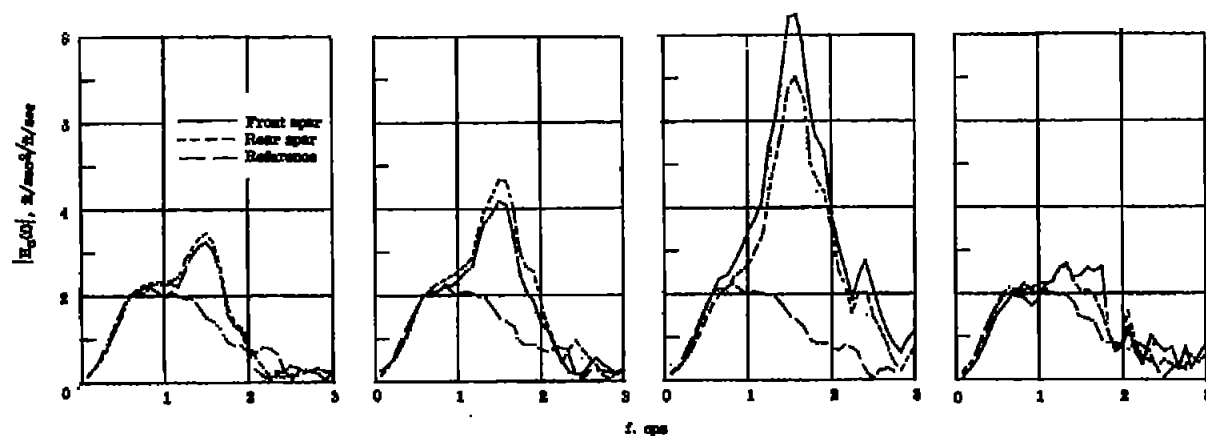
(a) Amplitude.
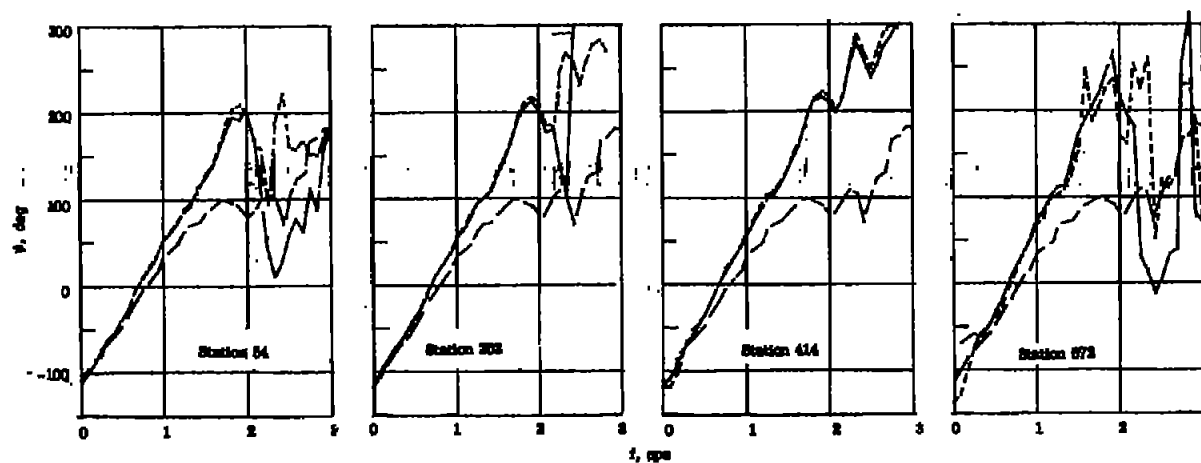
(b) Phase angle.

Figure 12.- Frequency-response functions of wing bending strain to vertical gust velocity for front and rear spars at four spanwise stations.
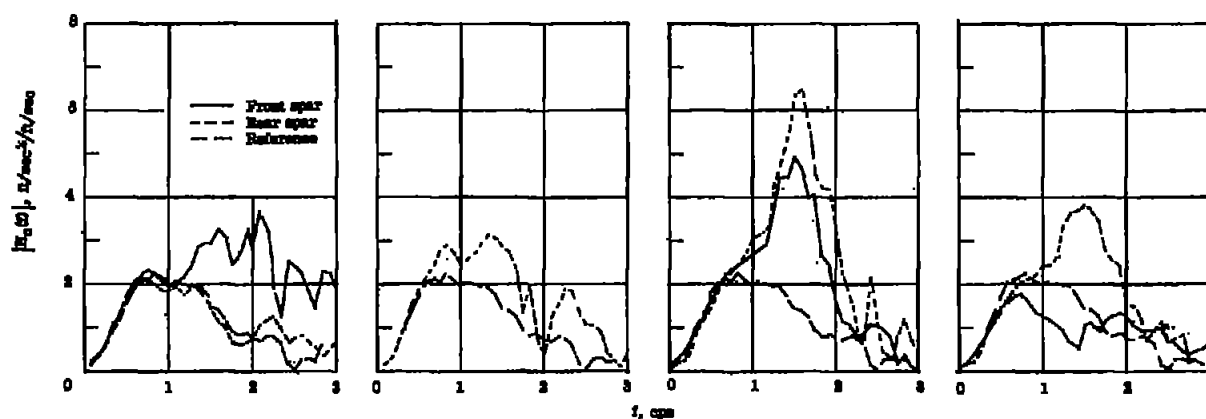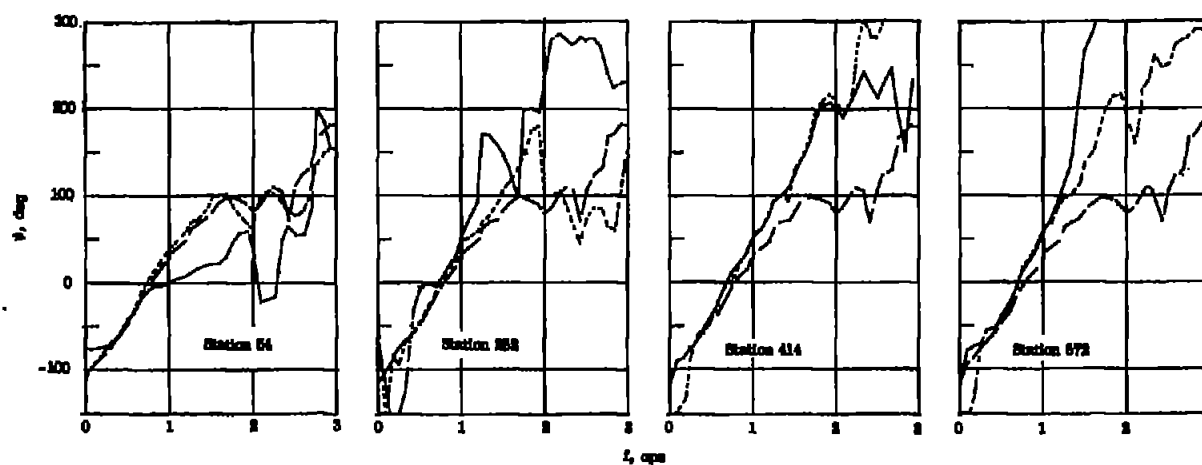
(a) Amplitude.

(b) Phase angle.

Figure 13.- Frequency-response functions of wing shear strain to vertical gust velocity for front and rear spars at four spanwise stations.
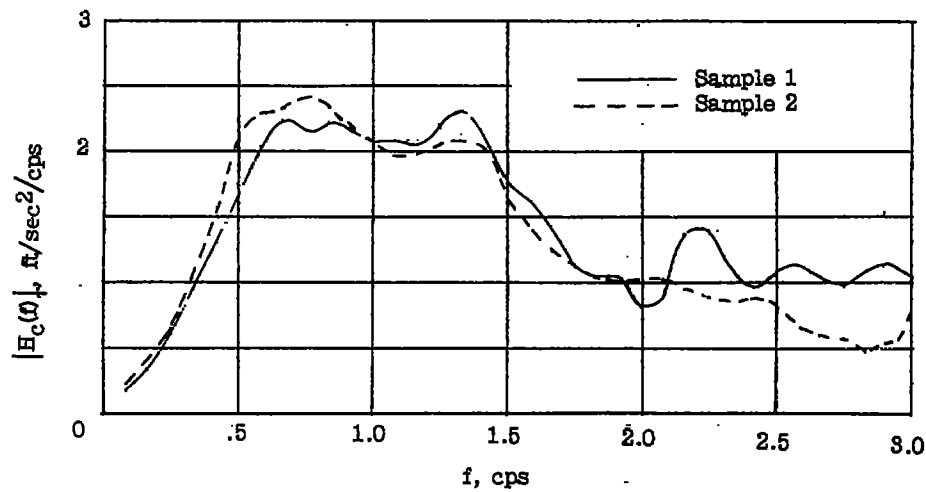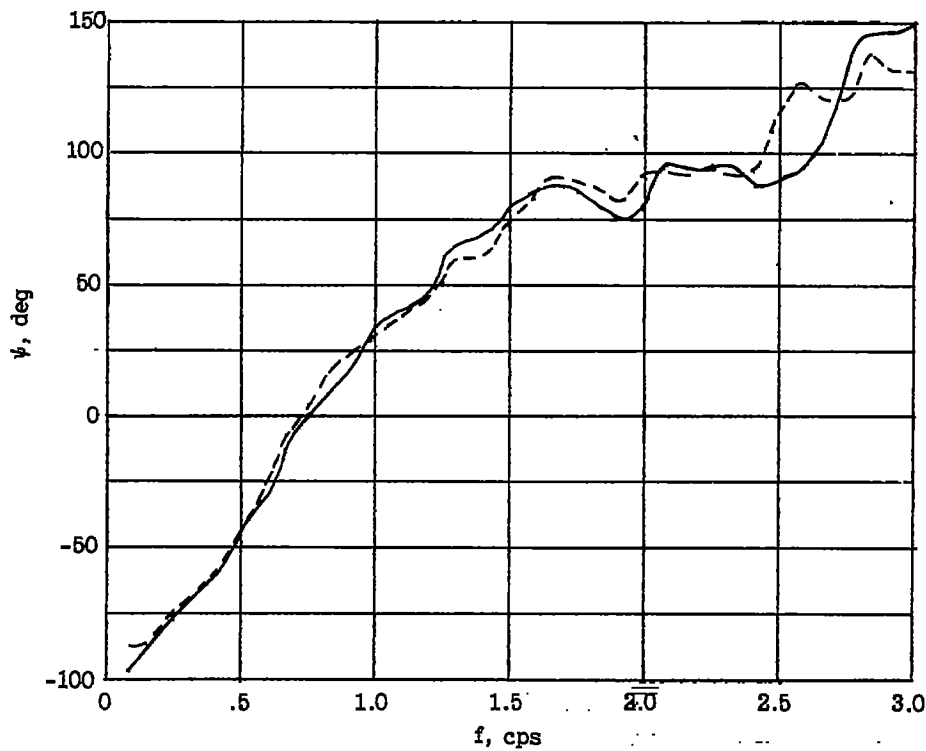
(a) Amplitude.

(b) Phase.

Figure 14.- Comparison of frequency-response functions of center-of-
gravity acceleration for two data samples of low-altitude tests.
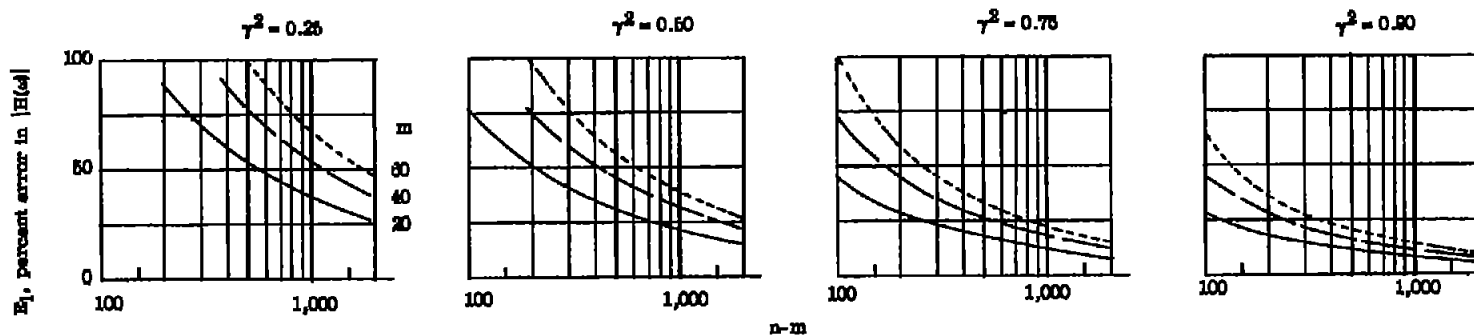
(a) Amplitude: confidence interval $= \left|H_C(\omega)\right| \Big/ \left(1 \pm \dfrac{E_1}{100}\right)$.
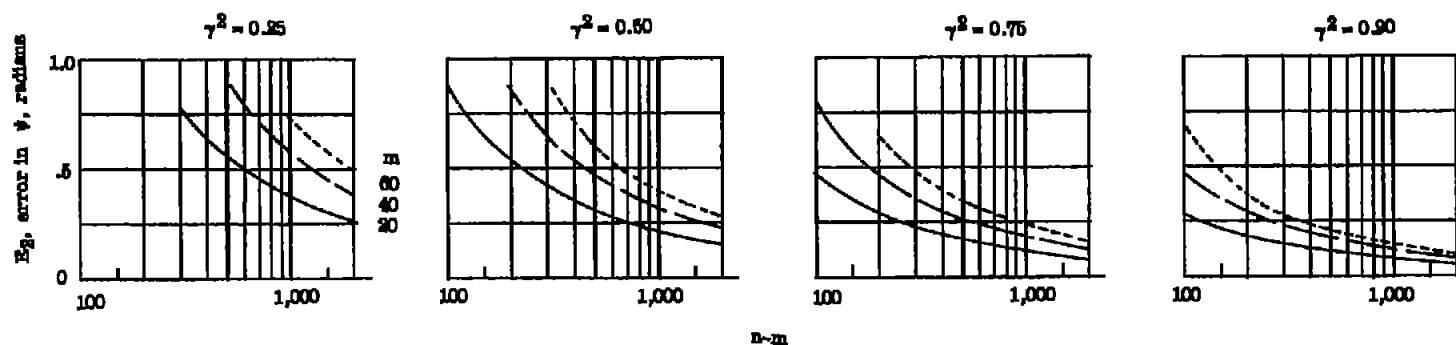
(b) Phase: confidence interval $= \psi \pm E_2$.

Figure 15.- Ninety-percent confidence intervals for amplitude and phase of estimates of frequency-response function.
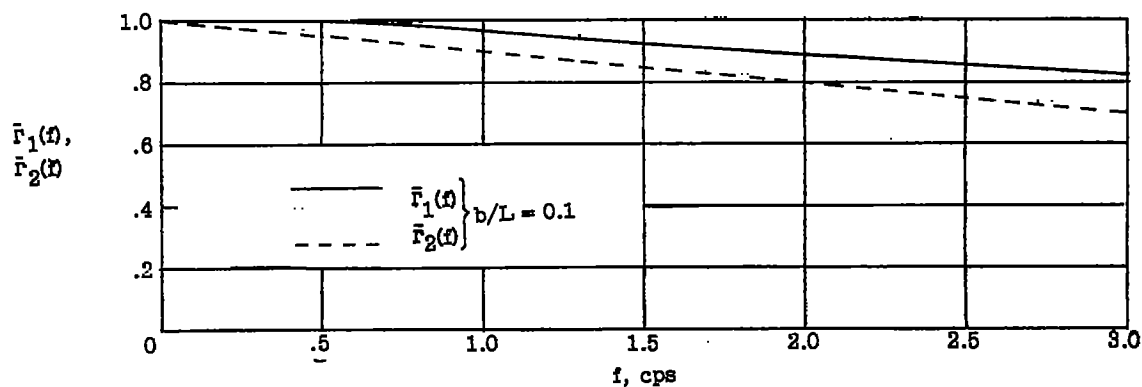
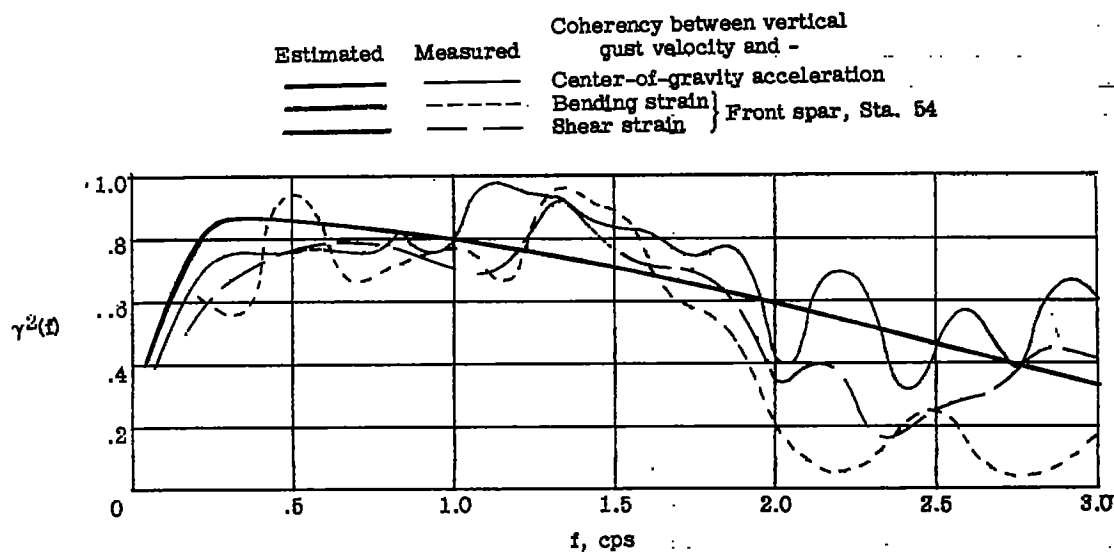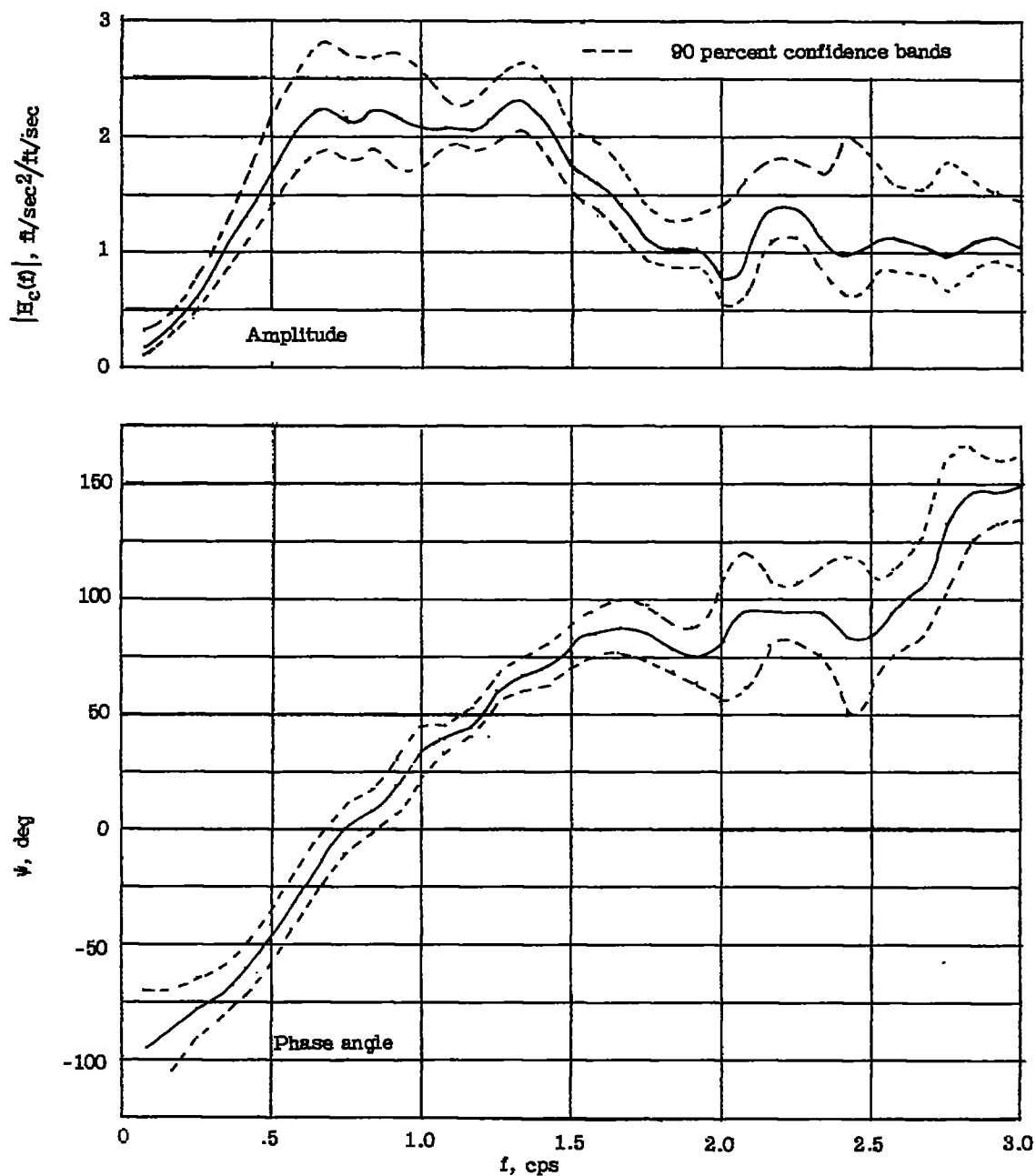Figure 16.- Span averaging functions $\overline{\Gamma}_1(f)$ and $\overline{\Gamma}_2(f)$.

Figure 17.- Comparison of estimated coherency functions between vertical gust velocity and airplane responses with measured results.

(a) Center-of-gravity acceleration.

Figure 18.- Statistical reliability of frequency-response functions of center-of-gravity acceleration and bending strain to vertical gust velocity.
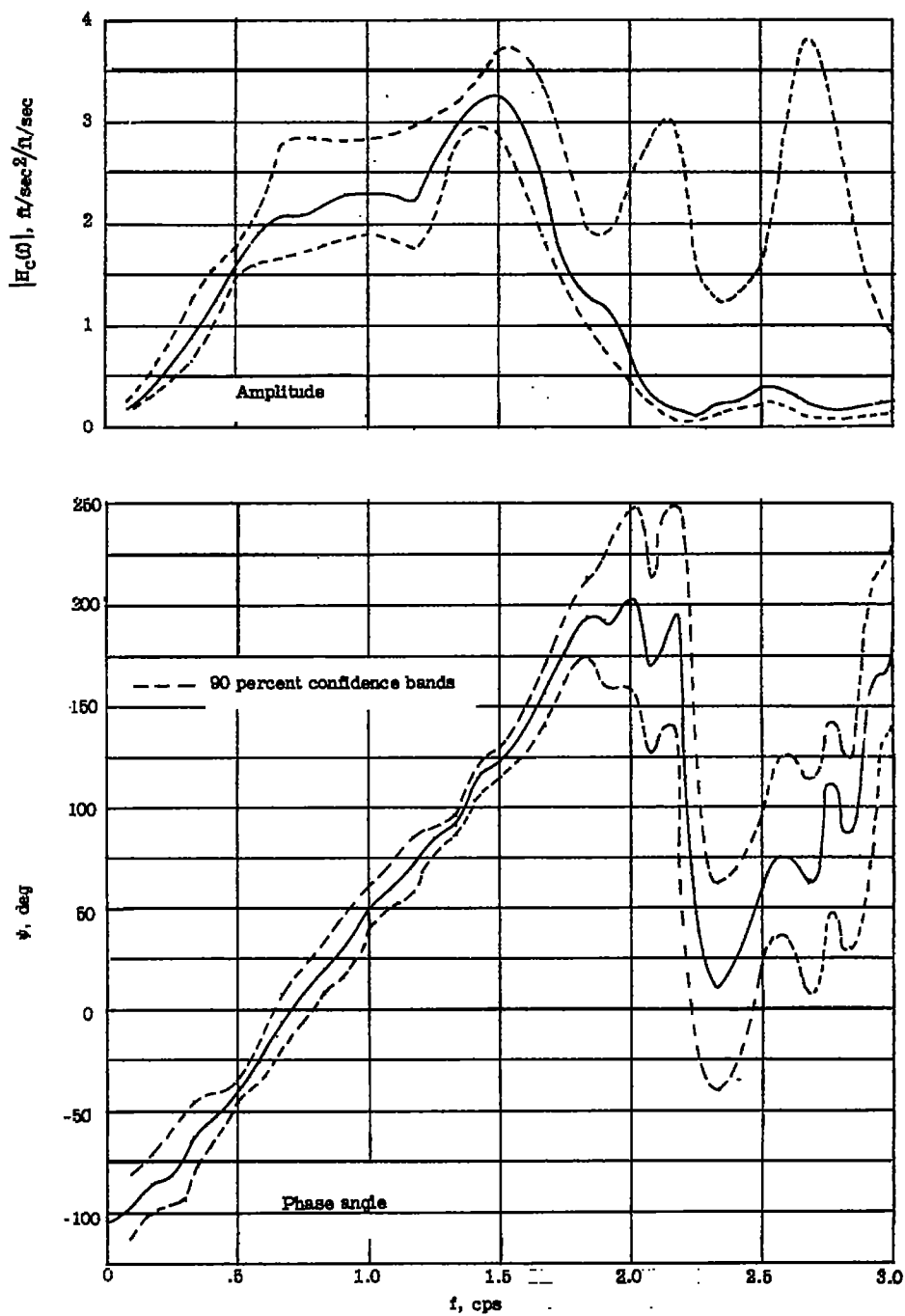
(b) Bending strain, front spar, station 54.

Figure 18.- Concluded.